Sedimentary Geology 455 (2023) 106479

Contents lists available at ScienceDirect

Sedimentary Geology

journal homepage: www.elsevier.com/locate/sedgeo

Morphological analysis of mineral grains from different sedimentary environments using automated static image analysis

Fruzsina Gresina [a,b,e,*], Beáta Farkas [d], Szabolcs Ákos Fábián [d], Zoltán Szalai [a,b,e], György Varga [a,c,e]

[a] Research Centre for Astronomy and Earth Sciences, Geographical Institute, Budapest, Hungary
[b] ELTE Eötvös Loránd University, Institute of Geography and Earth Sciences, Department of Environmental and Landscape Geography, Budapest, Hungary
[c] ELTE Eötvös Loránd University, Institute of Geography and Earth Sciences, Department of Meteorology, Budapest, Hungary
[d] University of Pécs, Institute of Geography and Earth Sciences, Department of Physical and Environmental Geography, Pécs, Hungary
[e] CSFK, MTA Centre of Excellence, Budapest, Konkoly Thege Miklós út 15-17., H-1121, Hungary

A R T I C L E I N F O

Article history:
Received 12 April 2023
Received in revised form 27 July 2023
Accepted 28 July 2023
Available online 7 August 2023

Editor: Dr. Catherine Chagué

Keywords:
Grain shape
Sediment transport
Micromorphology
Paleoenvironment
Granulometry
Granulometric proxy

A B S T R A C T

The properties of sediment grain shape provide valuable information about the transport mechanisms in different sedimentary and geomorphological environments. With the emergence of new, high-resolution analytical techniques, it has become possible to quickly examine the grain shape properties of a large number of individual mineral grains. In this study, we used automated image analysis (Malvern Morphologi G3SE-ID) to investigate mineral particles of four sediment types from different depositional environments (sand sheet (1), floodplain (2) and fluvial channel deposits (3), Pleistocene infilling material of sand wedges (4), $n = 20$) in the Carpathian Basin (Central Europe). Our primary objective was to identify quantitative key variables that can help objectively distinguish certain geomorphological environments located in the Carpathian Basin. In our analysis and data processing (which included techniques such as hierarchical cluster analysis, Wilks' λ, Kruskal–Wallis, multivariate analysis of variance and principal component analysis) we focused on four variables related to grain shape: circularity (form), convexity (surface texture), solidity (roundness) and elongation (form). The form of sedimentary grains depends largely on the physical properties of their source area, while the roundness depends on the energy of the transport medium and the distance of transportation. Surface texture or convexity can change in a relatively short time in a fluvial environment.

The study revealed that distinguishing geomorphological environments can be achieved by analyzing the circularity, convexity and solidity parameters of the sediment grains. Based on the established grouping, the analyses carried out with hundred repetitions showed that high sensitivity circularity, convexity and solidity variables were the most effective attributes regarding Kruskal–Wallis test statistics that provided significant ($p < 0.001$) results between the analyzed sedimentary environments, while the elongation was not able to provide significant results between the grouped samples. Statistical analyses of the MANOVA test with hundredfold repetitions showed significant differences between the derived groups. Wilks' λ test statistics and PCA showed that convexity and high sensitivity circularity discriminate the groups. Separate analyses of aeolian and fluvial sediments have been carried out. The Kruskal–Wallis analysis of variance showed the significant differences considering all four variables, and differences were also significant in the case of the MANOVA test. Wilks' λ test statistics and PCA showed that convexity, high sensitivity circularity and solidity discriminate the groups.

According to our results, the circularity parameter can provide information about the transport distance, while the solidity parameter can indicate the transport energy. The convexity parameter can serve as an indicator of both transport distance, as well as post-depositional processes. Some infilling materials underwent multiple transport processes, including high energy aqueous, wind transport mechanisms, and the post-depositional alteration process (frost weathering), while others originated from sand-sheet covered areas (active during Pleistocene glacials). The solidity parameter proved effective in separating sediments with similarly high convexity values (smooth surface), which were, in our case, from recent aeolian and fluvial environments. This result was due to the investigated fluvial sediments that inherited their form and low level of roundness from their source area. Our research supports that aeolian transport is more effective in rounding the grains than the aqueous environment.

Using automated static image analysis producing statistically stable results with hundreds of analyzed mineral grains provides useful indicators for paleogeographical reconstruction studies by investigating paleo and recent sediments.

* Corresponding author at: Research Centre for Astronomy and Earth Sciences, Geographical Institute, Budaörsi út 45, H-1112 Budapest, Hungary.
E-mail address: gresina.fruzsina@csfk.org (F. Gresina).

https://doi.org/10.1016/j.sedgeo.2023.106479

1. Introduction

Geomorphologists and geologists have long been interested in understanding the physical characteristics and relationship between various depositional environments, transportation processes and the general properties of the formed siliciclastic sediments (e.g., Udden, 1914; MacCarthy, 1935; Friedman, 1961; Visher, 1969; Middleton, 1976; Pye, 1995; Smalley et al., 2005; Vandenberghe, 2013; Vos et al., 2014). Over the past 100 years, sedimentary environments have been the subject of numerous publications, and sediments have been studied from many perspectives. One of the most popular approaches is the analysis of grain size and grain shape properties of sediments. The aim of these approaches was to identify and separate the different sedimentary environments from each other and to check the effects of multiple environmental influences (e.g., Vos et al., 2014; Woronko, 2016; Woronko and Pisarska-Jamrozy, 2016; Schulte et al., 2018; Varga and Roettig, 2018; Chmielowska et al., 2021; Kalińska et al., 2022; Martewicz et al., 2022). Reconstruction of transport mechanisms and distances, which probably played a role in the deposition, has also been a topic of previous studies (e.g., Mahaney and Andres, 1990; Costa et al., 2013; Woronko et al., 2015; Joo et al., 2018; Schulte et al., 2018; van Hateren et al., 2020; Chmielowska et al., 2021; Kalińska et al., 2022). Other common topics are climatic effects, which derive wind directions, wind and water flow velocity (e.g., Sun et al., 2002, 2004; IJmker et al., 2012; Kok et al., 2012; Krauß et al., 2016; Újvári et al., 2016; Katra and Yizhaq, 2017; Shang et al., 2018; Xu et al., 2018; van Hateren et al., 2020) and extreme transportation and deposition events (e.g. Parris et al., 2010; Mahaney and Dohm, 2011; Costa et al., 2012a, 2012b; Kalińska-Nartiša et al., 2018).

Mainly due to industrial needs, relatively new measurement techniques have also gained ground in environmental and earth sciences, opening new opportunities for high-resolution grain size and grain shape analyses, e.g., laser diffraction (Bieganowski et al., 2018; Bittelli et al., 2019; Varga et al., 2019a; Gresina, 2020), automated static image analysis (Sochan et al., 2015; Campaña et al., 2016; Lipiec et al., 2016; Varga et al., 2016; Joo et al., 2018; Varga and Roettig, 2018; Varga et al., 2018; Király et al., 2019; Chmielowska et al., 2021; Szmańda and Witkowski, 2021; Varga et al., 2021; Martewicz et al., 2022; Rostási et al., 2022), and dynamic image analysis (Altuhafi et al., 2013; Cosgrove et al., 2018; Shang et al., 2018; van Hateren et al., 2020), replacing the time- and sample-consuming methods, e.g., sieve and sedimentation methods (Konert and Vandenberghe, 1997; Beuselinck et al., 1998; Taubner et al., 2009; di Stefano et al., 2010; Bittelli et al., 2019; Gresina, 2020). The evaluation of sparse elemental number data on grain shape obtained by optical and electron microscopy has traditionally been based on subjective interpretation; therefore, comparability and reproducibility are relatively poor. However, electron microscopical microtextural high-definition investigations of grain surface properties are essential to precisely describe transportation mechanisms and post-depositional processes (Kuenen, 1959, 1960; Krinsley and Wellendorf, 1980; Costa et al., 2012a, 2012b, 2013; Vos et al., 2014; Woronko, 2016; Tunwal et al., 2018).

Applying mathematical–statistical methods has proven indispensable since processing a large amount of data is fundamental to exploring connections and drawing conclusions. Several ratio-based indicators, e.g., fine-coarse ratio, GSI, U-ratio (Keller, 1945; Doeglas., 1946; Bull, 1962; Passega and Byramjee, 1969; Vandenberghe and Nugteren, 2001; Rousseau et al., 2002), basic statistical descriptions and univariate to multivariate statistical analysis, e.g., hierarchical cluster analysis (Walling, 2013; Campaña et al., 2016; Kalińska-Nartiša et al., 2018; Varga et al., 2019b; Martewicz et al., 2022), linear discriminant analysis (Greenwood, 1969; Patro and Sahu, 1977; Chmielowska et al., 2021), principle component analysis (Vandenberghe et al., 1997; Costa et al., 2012a; Walling, 2013; Campaña et al., 2016; Kalińska-Nartiša et al., 2018; Chmielowska et al., 2021), end-member modeling (Prins et al., 2007; Dietze et al., 2012; Vandenberghe, 2013; van Hateren et al., 2018; Varga et al., 2019b; van Hateren et al., 2020) and parametric curve fitting methods (Sun et al., 2002, 2004; Varga et al., 2019b) were applied to distinguish between different transportation processes, energy levels or energy fluctuations of the transport medium. Consequently, granulometric proxies are widely used in paleogeographical and paleoenvironmental research.

The morphological characteristics of sedimentary particles can be interpreted as a granulometric proxy to provide insights into the physicochemical properties of the sediments. There are usually two approaches regarding particle shape: sorting by grain shape during transport mechanisms (e.g., Mazzullo et al., 1986; van Hateren et al., 2020) and changes in grain shape properties during transportation processes (e.g., Lewin and Brewer, 2002; Attal and Lave, 2009; Vos et al., 2014; Campaña et al., 2016; Chmielowska et al., 2021). We will discuss the latter in more detail, although the two mechanisms cannot always be clearly separated. There are three major aspects of the morphological description of grains (Barrett, 1980; Blott and Pye, 2008; Cox and Budhu, 2008; Tafesse et al., 2013). The form (Wentworth, 1922; Wadell, 1932; Krumbein, 1941; Folk, 1955; Sneed and Folk, 1958; Blott and Pye, 2008) is described by sphericity (circularity in 2D, Cox, 1927; Wadell, 1935; Riley, 1941), elongation and flatness, giving an overall geometrical expression of sediment particles (Barrett, 1980). The roundness (Wentworth, 1919, 1922; Wadell, 1932; Krumbein, 1941; Cailleux, 1942; Powers, 1953; Kuenen, 1959; Tafesse et al., 2013) is another approach to grain shape that gives an idea about the angularity level of the object. The third parameter is the surface roughness or surface texture (Kuenen and Perdok, 1962; Fitzpatrick and Summerson, 1971; Barrett, 1980; Woronko et al., 2015; Kalińska-Nartiša et al., 2018), which is a small-scale feature (Blott and Pye, 2008). Surface roughness is related to irregularity associated with the roundness level of the natural grains (Blott and Pye, 2008). Grain form, roundness and surface roughness can provide information about transportation mechanisms concerning the transport distance, transport energy and transport media (Kuenen, 1960; Helland and Holmes, 1997; Vos et al., 2014; van Hateren et al., 2020; Chmielowska et al., 2021).

Here, we explore and extend our knowledge of the granulometric proxies based on sediments' high-resolution objective granulometric parameters using automated static image analysis and multivariate mathematical–statistical methods to study thousands of individual mineral grains. Our approach is presented here by combining several particle shape parameters focusing on the following hypotheses: (i) we can explore statistical and mathematical analysis to detect differences between sedimentary environments in the Carpathian Basin; (ii) we can deduce modes of transport (relative distance, time and energy); (iii) as a result of the preceding, it is possible to separate such sediments, which have been a major challenge in granulometric environmental reconstruction studies (e.g., fluvial and aeolian sediments).

2. Materials and methods

2.1. Samples

We investigated sand samples from spatially and temporally various geomorphological environments of the Carpathian Basin, Central Europe. The granulometric analyses were based on filling material from Late Pleistocene periglacial sand wedges and sand-sized grains from a recent aeolian sand sheet, fluvial bedload and floodplain sediments (Table 1, Figs. 1, 2).

The filling material of sand wedges was sampled from two main sample areas ($n = 9$). For details on the formation of frost cracks, see, Black (1976), Vandenberghe and Pissart (1993), and Murton et al. (2000). Samples are from the sand-filled polygonal crack network (P9–P39) in Kemeneshát, where Pliocene cross-bedded fluvial sands overlay the Upper Miocene lacustrine sediments and then by the old gravel layer of the Rába river (Somogyi, 1962) and the cryoturbation forms were described in relict reddish brown forest soils (for details

Table 1
Investigated sediments from the Carpathian Basin. Alsóújlak, Csipkerek, and Szemenye are located in Kemeneshát polygonal network. DTI = Danube–Tisza Interfluve.

Sample code	Lab code	Field code	Location	Coordinate (latitude)	Coordinate (longitude)	Environment	Depth
Nyírség	150744	NYIR1	Debrecen	47.527778	21.729472	Sand sheet	0–10 cm
DTI 1	210131	20210220	Fülöpháza	46.900000	19.400000	Sand sheet	0–10 cm
DTI 2	210132	20210220	Fülöpháza	46.900000	19.400000	Sand sheet	10–20 cm
DTI 3	210133	20210220	Fülöpháza	46.900000	19.400000	Sand sheet	20–30 cm
DTI 4	220032	106	Jakabszállás	46.747944	19.573806	Sand sheet	0–10 cm
DTI 5	220034	117	Jakabszállás	46.747944	19.573806	Sand sheet	10–20 cm
Maros	160038	MAR1	Makó	46.218361	20.381083	Channel deposit	0–10 cm
Danube 1	210134	20210301	Dömös	47.760000	18.910000	Channel deposit	0–10 cm
Danube 2	210135	20210301	Dömös	47.760000	18.920000	Channel deposit	0–10 cm
Dráva 1	220030	42/4	Drávasztára	45.805654	17.831412	Channel deposit	0–10 cm
Dráva 2	220031	170/1	Barcs	45.967395	17.330969	Floodplain	0–10 cm
P10	P10	Au1/3	Alsóújlak	47.074017	16.851633	Sand wedge infilling	
P13	P13	A2/2	Alsóújlak	47.074017	16.851633	Sand wedge infilling	
P32	P32	A1/2	Alsóújlak	47.074017	16.851633	Sand wedge infilling	
P28	P28	CS6	Csipkerek	47.08854	16.90517	Sand wedge infilling	
P39	P39	CS3	Csipkerek	47.08854	16.90517	Sand wedge infilling	
X3	X3	X-3	Mogyoród	47.583333	19.216667	Sand wedge infilling	
P9	P9	SZ6/6	Szemenye	47.080318	16.908085	Sand wedge infilling	
P21	P21	SZ7/2	Szemenye	47.080318	16.908085	Sand wedge infilling	
P29	P29	SZD1/C	Szemenye	47.080318	16.908085	Sand wedge infilling	

see Fábián et al., 2014; Farkas et al., 2023). In the gravel quarry of the Mogyoród sand sample (X3, Gödöllő Hills), yellowish–reddish paleosols were deposited on the old Danube gravels, which were dissected by polygonal fractures filled with sand (Kovács et al., 2007; Fábián et al., 2014). Gödöllő Hills' W–NW margin is built up by Miocene sandstone and gravel formations. To S–SE of the latter, Upper Miocene sandy, clayey sediments and alluvial sediments are deposited by Ancient Danube and northern rivers (Dövényi, 2010).

The samples from aeolian sand sheets (n = 6) were taken from the sandy areas of the Danube–Tisza Interfluve (DTI) area (Sandhills of Kiskunság: Fülöpháza, Jakabszállás; DTI1–5) and the Nyírség (South-Nyírség: Debrecen; Nyírség). The origin of the windblown sands of the

Fig. 1. Geographical distribution of the investigated sand sediments.

DTI is linked to the Upper Plio-Pleistocene alluvial fans of the former northwest–southeast flow of the Danube, which were deposited on the Upper Miocene sediments (Gábris et al., 2012). Periods of sand movements were recognized during the last 25 ka (Gábris et al., 2012).

During the Late Pleistocene, the Nyírség alluvial fan was uplifted while the surrounding regions were sinking, influencing the rivers, which shifted gradually down. The fluvial deposits had been placed in a prominent dry position creating opportunities for wind to blow out the sand in dry periods (Lóki et al., 1994; Buró et al., 2016). Periods of sand movements were recognized between the last 27 and 22 ka (Buró et al., 2016).

The sand from the riverbeds and floodplains was provided by the Danube (Danube Bend, n = 2; Danube 1, Danube 2), Dráva (Dráva Plain, n = 2; Dráva 1, Dráva 2) and Maros rivers (Marosszög, n = 1; Maros). The Danube's recent fluvial sediment originates from the Danube Bend, which is geographically defined as an antecedent erosion valley spatially between Visegrád and Börzsöny Hills composed of mid-Miocene volcanic succession (Ruszkiczay-Rüdiger et al., 2005). The studied recent sediment of the Dráva is derived from a middle-course fluvial environment. Much of the landscape surface is a floodplain, but abandoned meanders are typical in flood-free areas (Dövényi, 2010). The third member of the fluvial sediment trio is derived from sediment transported by the anastomosing Maros River. The Marosszög area's gradual refinement of the Holocene sedimentary sequence from bottom to top indicates a steady decline in the carrying capacity of the Maros River (Dövényi, 2010).

The samples were selected to demonstrate the instrument's ability to detect differences in the shape characteristics of sand grains from different sedimentary environments. With this approach, the method can subsequently be applied to more detailed sediment analyses, such as a complete sand sheet, dune profile and buried sediments. The aim was therefore not to examine a single sedimentary environment in detail, but to compare them and select which morphological variables are suitable for differentiating between sediments. It is therefore assumed that 20 samples are sufficient.

2.2. Automated static image analysis

Automated image analysis techniques can provide a statistically robust, objective, and representative sample description by a large number of observed grains. The mineral grains were scanned using the 5× objective to provide a 0.56 μm pixel size of the built-in Nikon Eclipse microscope and CCD camera of the Malvern Morphologi G3SE-ID device (Malvern Panalytical, Malvern, Worcestershire, UK) under transmitted (diascopic) illumination providing 0.3 μm^2/pixel resolution. The system takes multiple pictures of the dispersed grains at different focal heights (three layers above and two below the focal plane, equivalent to 244 μm in total) and then merges them to store the scanned individual grains as a single, 2D grayscale image. Not only the size distribution of the grain populations is determined, but also the distribution of different shapes (e.g., circularity, convexity) and other shape-dependent size parameters (e.g., circular equivalent diameter, length, width, circumference, area) of each grain. The automatically calculated values of different shape properties usually take a value between 0 and 1 on a scale of 1001 units with an increase of 10^{-3}.

The Morphologi G3SE-ID instrument can provide chemical analysis of samples using a Raman spectrometer (Kaiser Optical Systems Raman Rxn1 Spectrometer, 785 nm, <500 mW) in addition to standard morphological analysis. We applied 5 s for particle exposure with three numbers of Co-Adds using high laser power. We targeted an average of 100 mineral grains per sample to describe their qualitative mineral properties.

Regarding our research, particle shape is treated synonymously with grain morphology; we consider these two terms as a broad external expression of the natural grains containing form, roundness and surface texture. Here, we define circularity and elongation as a description of the form of the grains (Blott and Pye, 2008), although convexity and solidity are related to the roundness level of the particles (Chmielowska et al., 2021). Moreover, convexity also provides information about surface texture (Campaña et al., 2016; van Hateren et al., 2020). Fig. 3 describes the interpretation of the formulas for the shape parameters. The interpretation of circularity, convexity, solidity and elongation/aspect ratio as a function of transport processes is perhaps the most widely used indicators for determining transport conditions (e.g., Suzuki et al., 2015; Joo et al., 2018; van Hateren et al., 2020; Chmielowska et al., 2021; Szmańda and Witkowski, 2021; Varga et al., 2021; Martewicz et al., 2022). A more

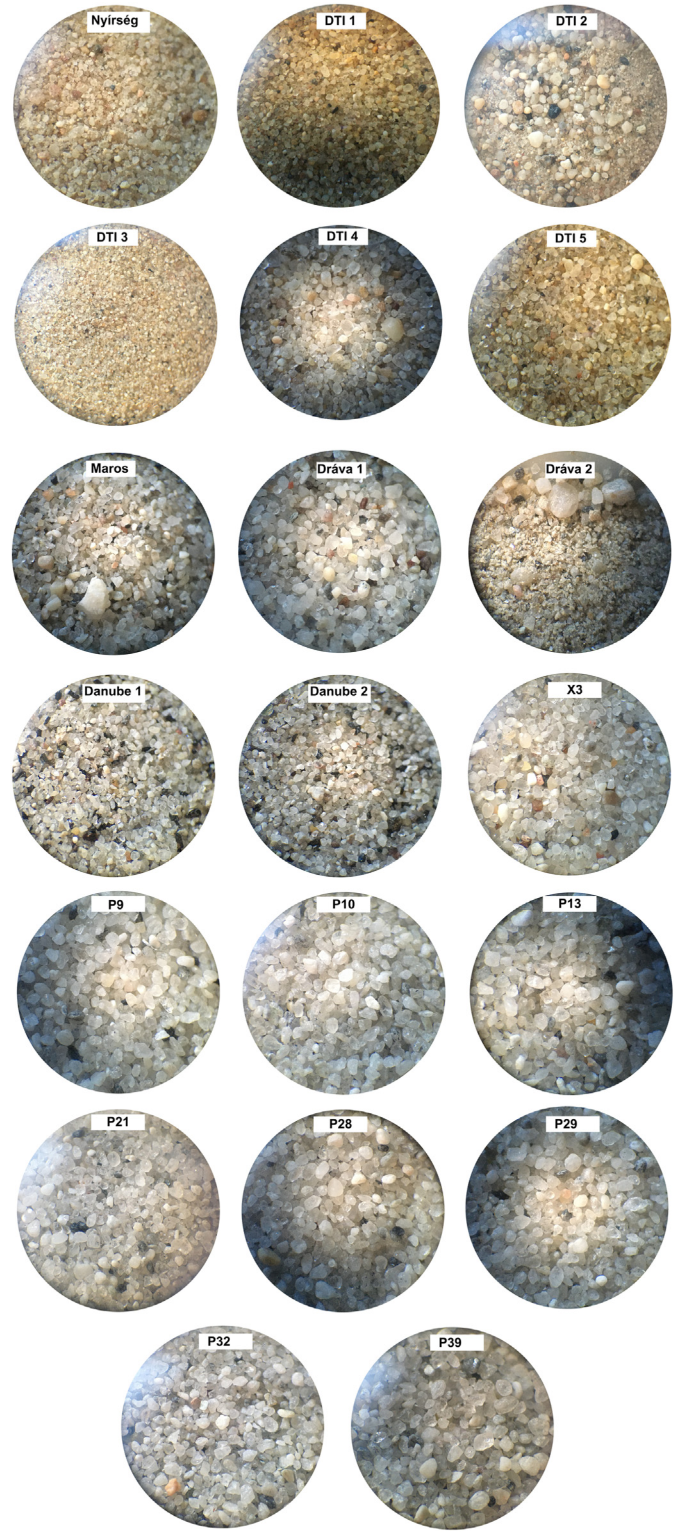

Fig. 2. Photographs of the investigated samples.

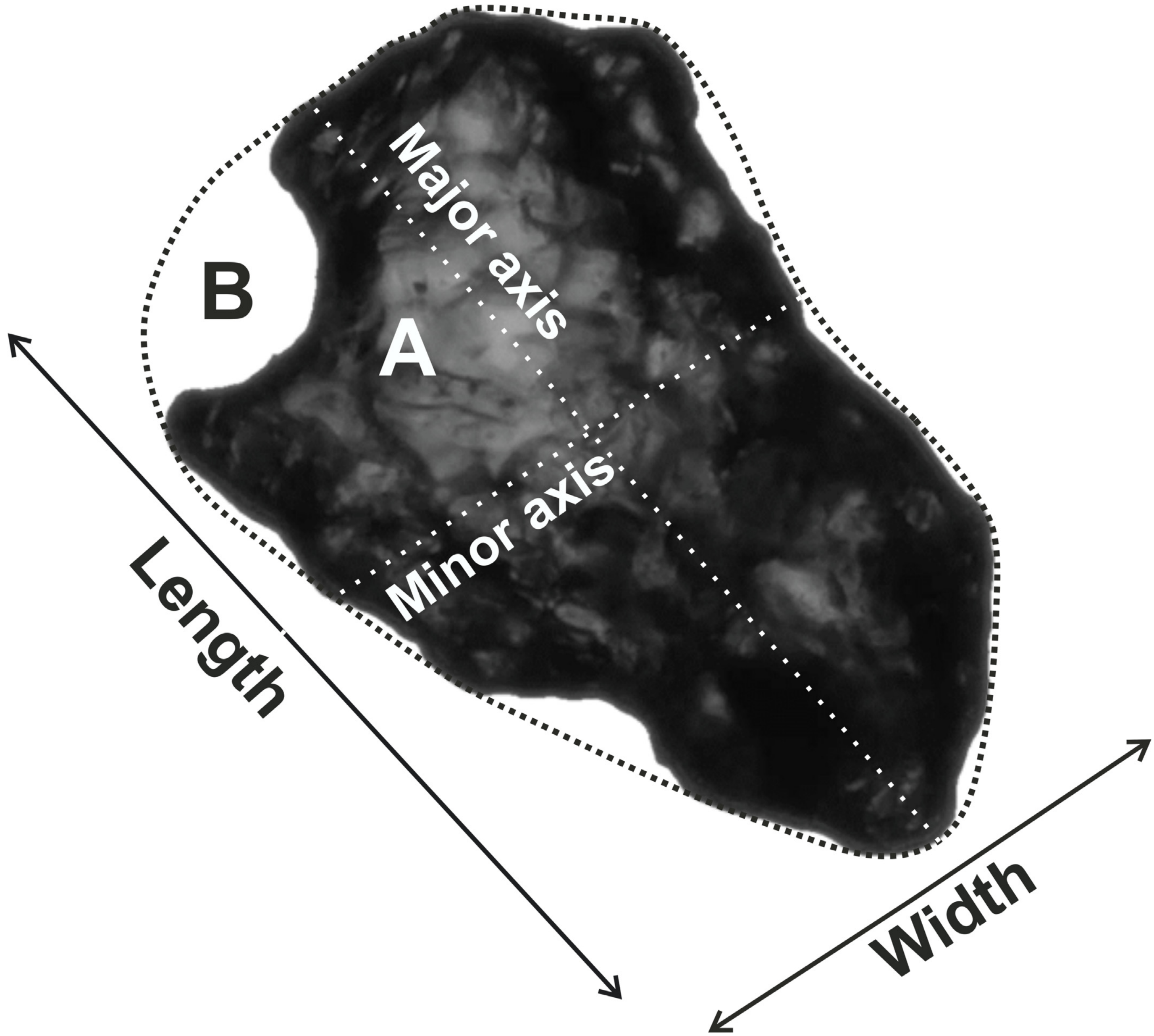

Fig. 3. Illustration to interpret the grain shape formulas. A = area of the particle; B = area of the convex hull.

accurate indicator of the circularity property is the high sensitivity (HS) circularity, which is calculated by the instrument as the ratio of the projected area of the grain to the square of its circumference:

$$HS\ circularity = (4 \times \pi \times Area)/Perimeter^2$$

The value of convexity is determined by dividing the circumference of the convex hull by the circumference of the grain. The perimeter of the convex hull is the smallest convex polygon containing the area of the grain (perimeter of A + B):

$$Convexity = (Perimeter\ of\ A + B)/Perimeter\ of\ A$$

The degree of grain solidity (the amount of depression or protrusion) is given by the ratio of the area of the investigated object to the area enclosed by the convex hull:

$$Solidity = A/(A + B)$$

As a definition, the aspect ratio is given by the ratio of the width to the length of the tested grain. If this result is interpreted as the difference between the value obtained and 1, a more accurate characterization of the elongation of the grain is obtained:

$$Aspect\ ratio = Width/Length$$

$$Elongation = 1 - (Width/Length)$$

2.3. Sample pretreatments

Before the grain shape analysis of the mineral particles, applying chemical pretreatment procedures is inevitable, considering the aggregation effect of organic matter and calcium carbonate (Battarbee et al., 2001; Vaasma, 2008; Gray et al., 2009; Cosgrove et al., 2018; Varga et al., 2019a; Gresina, 2020). The presence of aggregates can give false results if they are interpreted as individual grains. Due to the novelty of the automated static image analyzer, no generally accepted method has yet been developed for the pretreatment of sediments.

We weighed 5 g of sediment into a 50 mL centrifuge tube and added 5 mL of 30 % H_2O_2. We cured the samples for 24 h, then heated them to 60 °C. We repeated the procedure by adding a small amount of reagent to detect if there was any reaction. We heated the sample to decay the H_2O_2. After cooling, the tubes were filled with distilled water, centrifuged for 15 min at 3500 rpm, and then washed with distilled water. For calcium carbonate removal, we used 10 % HCl. We added at first 5 mL HCl to the previously degraded and washed sample. We cured the sample with a reagent for 24 h, then heated it to 60 °C. We added additional reagents depending on whether there was still a reaction. We centrifuged the solution, pipetted the supernatant and refilled the tube with distilled water. We repeated this process until the pH was neutral.

2.4. Data processing

Approximately, 50 mm^3 of grains was dispersed on the glass plate by compressed air and the device scanned about 2000–5000 grains per sand sample. This amount provided us with 500–1500 analyzable grains per sample after post-processing and filtering. The filtering criteria included removing overlapping grains, incomplete images, and grains representing non-mineral grains (e.g., fibers). It has to be noted, that the compressed air scatters the sediment grains onto the glass plate so that the largest area of the particles is facing the camera. However, this is only one result among an infinite number of possible projections of a three-dimensional object. The major drawback of static automated image analysis is the unknown thickness of particles (Varga et al., 2018). In measurements using dynamic image analysis techniques, such particle orientation problems do not distort the results, since free-falling particles are free to rotate in all directions (Shang et al., 2018).

Based on Raman spectroscopical investigation, the quartz dominance was above 90 % per sample. The grains below 10 μm were also removed from the database because the smaller particles have a smaller area covered by pixels, which can lead to simplified shape properties compared to larger grains (Varga et al., 2018; Varga et al., 2019a; Gresina, 2020). The distributions of shape properties were analyzed based on the volume weighting of the data. Image analysis grain size results indicated an underestimation of clay and fine silt fractions compared to laser diffraction measurements, while the modal values of the coarse silt (or fine sand) fraction were found to be higher than those obtained by laser particle sizing (Varga et al., 2018). The knowledge of the third dimension is more necessary for platy grains regarding their true size (e.g., clay, mica). In our case, that is why we have analyzed the 250–500 μm size fraction, which contains rather large and relatively spherical grains, we are certainly investigating sands even with overestimation. Then we randomly selected 100 × 100 grains per sample from the 250 to 500 μm grain size fraction. We tested a hundred times for significance and used the averaged values for visualization, also in descriptive statistics.

Besides Pearson correlation and descriptive statistical analysis, we applied univariate and multivariate data processing methods. We applied hierarchical cluster analysis to classify the sediments, resulting in three classes using Euclidean distances and average linkage. We investigated the Wilks' λ values of the four morphological variables. A univariate analysis method like Kruskal–Wallis analysis of variance was performed using $\alpha = 0.05$. We analyzed the classified data by multivariate analysis of variance (MANOVA) using $\alpha = 0.05$ after data normalization. We applied the results from MANOVA, like canonical variables and multivariate test statistics. Principal component analysis (PCA) was performed to determine which shape-related variable describes the different groups and sedimentary environments. The data analysis procedures and visualization of these results were performed in the MATLAB environment.

3. Results

3.1. Grain size and shape distribution

According to the grain size distribution curves of sand wedge materials (Fig. 4a), there are differences between the samples on modes that distribute between 343 and 453 μm (Table S1). The P9 has the smallest, and P39 has the largest mode. The grain size distributions of fluvial samples also have differences regarding modes. Modes range between 252 and 653 μm (Fig. 4b; Table S1). The smallest modes belong to the

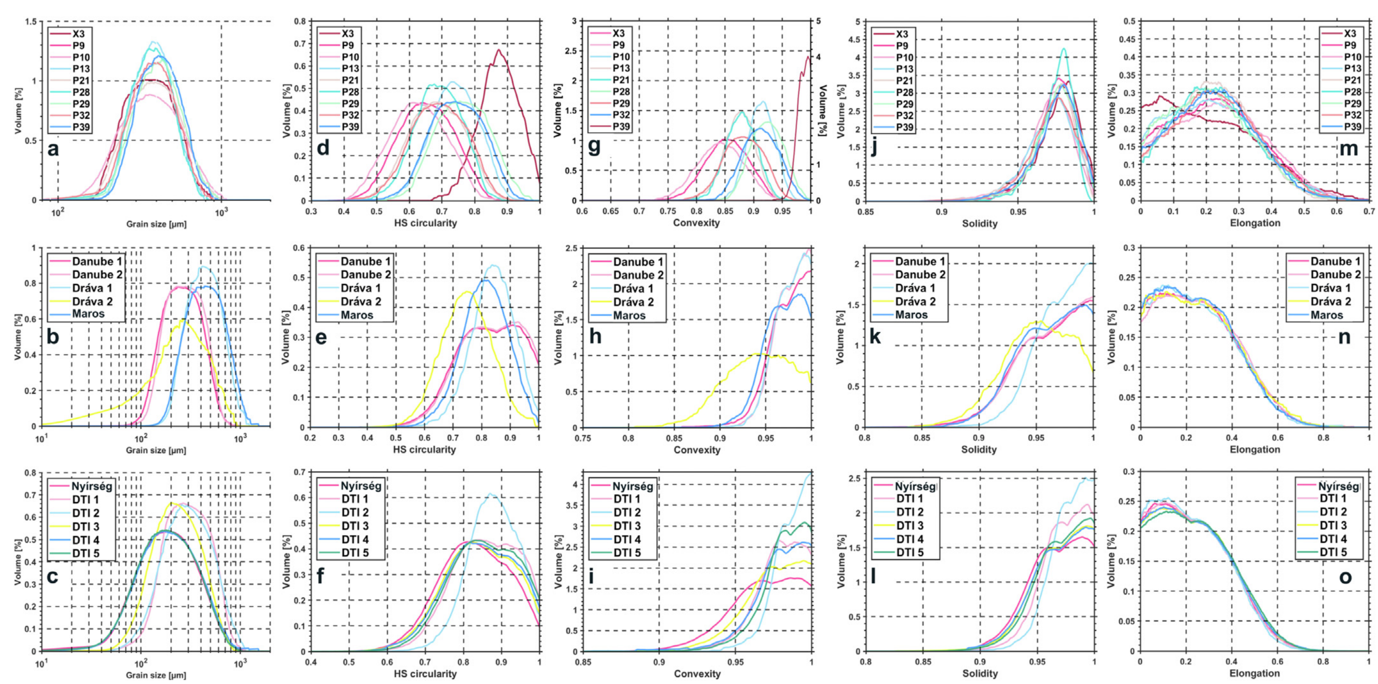

Fig. 4. Distribution curves of grain size, HS circularity, convexity, solidity and elongation. 1st row = filling material of sand wedges; 2nd row = fluvial sediments; 3rd row = aeolian sediments; 1st column = HS circularity; 2nd column = convexity; 3rd column = solidity; 4th column = elongation. Grain size data was measured by automated static image analysis. HS circularity = high sensitivity circularity.

Danube (310 μm, 252 μm) samples, and the largest values are from the Dráva riverbed (Dráva 1, 653 μm) sample. The aeolian samples have grain size modes between 210 and 346 μm (Fig. 4c; Table S1). The samples from Fülöpháza (DTI 1–3) have larger values regarding modes than sediments from Nyírség and Jakabszállás (DTI 4–5). The filling material of sand wedges has modes an average of 394 μm, which is between the mode values of aeolian and fluvial samples.

The grain shape distribution curves provide a more detailed visual separation (Fig. 4d–o). According to HS circularity, the distribution curve of X3 has the highest values and is very distinct from other samples within the sand wedges (Fig. 4d). The P13, P29 and P39 samples have relatively high values compared to the other sand wedge sediments — the lowest values related to P10 and P9. The HS circularity results of the fluvial samples show differences in the Maros and Dráva sediments (Fig. 4e). The Dráva's floodplain sediment (Dráva 2) shows a less regular feature than the other fluvial and aeolian sediments. The Danube sediments contain regular grains compared to other fluvial samples and show very similar circularity values compared to each other. The aeolian samples show fewer differences than the fluvial ones in terms of their shape distribution. The Nyírség sample indicates a relatively lower circularity result (Fig. 4f). The rest of the sediments have similar curves.

The convexity variable shows the same trend as HS circularity values (Fig. 4g–h–i; Table S1). The infilling material of sand wedges has the same characterization as circularity results. The most convex grains are in the X3 sample (mode = 0.990), and the least convex particles are in P9 and P10 sediments (mode = 0.842; mode = 0.832). However, the average value of P9 is above 0.9. Within the group of fluvial sediments, the floodplain sample (Dráva 2, mode = 0.953) is less convex. Within the other fluvial samples, the least convex grains are in the Maros sediment (mode = 0.973). According to the aeolian samples, the Nyírség sediment shows a less convex image with the mode of 0.977. The most convex character belongs to the DTI 2 sample.

The solidity feature of the investigated sand wedge samples does not show striking differences (Fig. 4j–k–l; Table S1), although slightly distinctive values can be established among them. The lower values are linked to P9, P10 and P32 sediments (mode = 0.978; mode = 0.978; mode = 0.979). The other samples from that type of sediments have modes above 0.98. Among the fluvial samples, the lowest solidity values are connected to Dráva 2 (mode = 0.937). The rest of the fluvial sediments have similar values on the solidity property. The modes range between 0.960 and 0.969. Half of the aeolian samples have solidity modes above 0.983 (DTI 2, DTI 3, DTI 5). The other aeolian sediments have 0.970–0.975 (Nyírség, DTI 1, DTI 4).

The last analyzed variable is elongation (Fig. 4m–n–o). Visually this variable is the most difficult to analyze and distinguish among the samples tested. Within the sand wedge materials, the X3 sample has a very different mode (0.08; Table S1). The largest mode on the elongation shape property is related to P10 (0.325). The fluvial sediments show differences; the greatest value is linked to Maros (mode = 0.281), while the lowest values are regarded to Dráva samples (mode = 0.142; mode = 0.156). The aeolian samples have diverse results. The highest elongation value is linked to Nyírség (mode = 0.257) and DTI 3 (mode = 0.238). DTI 2 and DTI 4 have values near zero (Table S1).

3.2. Statistical analyses of grain shape properties

3.2.1. Descriptive statistics

Statistical analyses were performed on 100 × 100 grains from each of the 20 investigated samples. We applied basic descriptive statistics of the four grain shape properties averaged over 100 × 100 grains (Table S2). According to the values of HS circularity, the lowest mean values are related to P9 and P10, the highest to X3 and samples from the Danube–Tisza Interfluve. Although, the fluvial samples show relatively low mean values (Dráva 2, Maros, Danube 1, Danube 2). The standard deviation (STD) ranges from 0.044 to 0.069. The lowest value is from DTI 2, and the highest is from Danube 1. The maximum values above 0.9 are related to aeolian and fluvial samples except Dráva 2. Samples from the filling material of sand wedges do not contain any grains above the value of 0.9. The lowermost minimum values are related to the sand wedges and some fluvial samples (Maros, Danube 2, Dráva 2).

The filling material of sand wedges shows low values of convexity compared to fluvial and aeolian samples; the exception is X3. Among the sand wedge samples from Kemeneshát, the highest mean values related to P39, P13, and P29 and the lowest are P9 and P10. The STD values are lower within every sample than were in the case of HS circularity. The maximum values almost reach 1.00 within aeolian samples. Among the sand wedge samples, the highest values were linked to X3 and P39, P13, and P29. The lowermost values from minimum are related to the sand wedges and some of the aeolian and fluvial samples (Danube 1, Dráva 2, Maros).

The solidity variable distinguishes the sediments differently. The highest mean solidity values are linked to aeolian and sand wedge materials with values above 0.967, and the lowest results are related to fluvial samples below 0.967. The STD results show relatively high values based on fluvial samples. The maximum values do not differentiate the sediments.

The highest values from the elongation mean are linked to Maros, Danube 1 and Danube 2 fluvial sediments and P13, P28, and P39 sediments. The lowest values from this variable are related to X3. In general, the STD results are very high compared to the other three shape variables. The highest maximum values are linked to Danube 2, Maros, and Danube 1 and P28, P29, and P39.

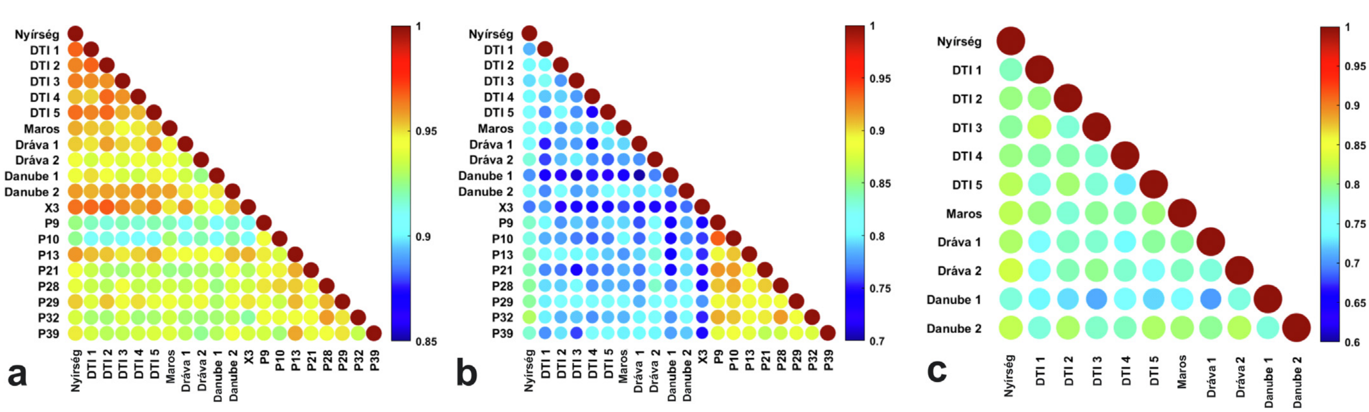

Fig. 5. a–b: Pearson correlation plot of all investigated sediments based on (a) four and (b) three grain shape variables. c: Pearson correlation plot of fluvial and aeolian sediments based on three grain shape variables. DTI = Danube–Tisza Interfluve.

3.2.2. Linear correlation analysis

Based on Pearson correlation analysis of all four grain shape variables, the correlation coefficient is above 0.9 between the sediments (Fig. 5a). The P9 and P10 samples stick out of the dataset. They correlate well with each other and with other sand wedge sediments in comparison to aeolian sediments. The X3 Mogyoród sample's correlation coefficient converges to 1.0 for aeolian sediments. The fluvial and aeolian samples cannot be separated from each other or the filling material of sand wedges besides the two distinctly differentiated sediments (P9, P10).

The correlation plot of Fig. 5b shows that the three investigated variables changed the results of correlation coefficients among the sediment samples. The correlation between the infilling materials of sand wedges is much higher (0.9) than among aeolian samples (0.75). The X3 sample's results show a relatively low correlation coefficient between aeolian sediments compared to the investigation of four variables. Dráva 2 and Nyírség aeolian samples show a 0.8–0.85 correlation coefficient value between most sand wedge materials. The fluvial samples show a 0.8 correlation coefficient among them.

According to the correlation plot of the aeolian and fluvial samples (Fig. 5c), the correlation coefficients are lower than when we investigated all four variables. However, the correlation between fluvial samples is higher (0.8–0.85) than among aeolian samples (0.75).

3.2.3. Hierarchical cluster analysis, Wilks' λ

Hierarchical cluster analysis classified the sediments into three classes based on four variables (Fig. 6a). The 1st group (pink) contains all aeolian samples, the four (out of five) fluvial samples and the X3 sand wedge sample. The 2nd group (green) has the remaining fluvial sample (Dráva 2) and P13, P29, and P39. The 3rd group (blue) has the remaining sand wedge sediments, P10, P9, P28 and P39 samples. The analysis of Wilks' λ of certain variables (Fig. 6a1) shows that the most influential variable is the convexity ($\lambda = 0.2371$). The scatter plot of the variables (Fig. 7a) helps to determine which variables can be used to separate the groups and samples. A possible linear relationship between two variables is between HS circularity and convexity.

We analyzed the aeolian and fluvial samples ($n = 11$) using HS circularity, convexity, solidity and elongation parameters. According to the hierarchical cluster analysis, four separate fluvial groups were made (Fig. 6b). However, preliminary Kruskal–Wallis suggests that the samples Danube 1–2, Maros and Dráva 1 belong to the same group ($\alpha = 0.05$; $p_{HSC} = 0.2$; $p_{conv} = 0.67$; $p_{sol} = 0.76$). Therefore, further analyses were carried out with these three groups: 1st group (pink) contains aeolian samples, 2nd group has the four fluvial samples (green), and the 3rd group (blue) has only the Dráva 2 floodplain sediment. The investigation of Wilks' λ (Fig. 6b2) shows that three variables influenced the results. The solidity variable had a more significant impact on the results than in the case of the previous grouping.

3.2.4. Analysis of variance

We analyzed the four shape variables one by one with Kruskal–Wallis tests using the classification from the cluster analysis (Fig. 8). According to the HS circularity, convexity and solidity results by the first grouping method, the three groups significantly differ from each other, which is further represented by the p-value (Fig. 8a–c). For elongation variables (Fig. 8d), the p-value is above 0.05. The null hypothesis cannot be rejected because the results indicate that all group means are equal. The Kruskal–Wallis results on hundredfold repetition were the same as above. The results on HS circularity, convexity and solidity were 100 % significant and the elongation variable was never significant.

The fluvial and aeolian sediment groups transformed from cluster analysis have also been applied to Kruskal–Wallis (Fig. 8e–h). The box plots show that the groups can be distinguished based on all four variables according to p-values; Kruskal–Wallis rejects the null hypothesis that all group means are equal. The results of hundredfold repetition on the Kruskal–Wallis test for HS circularity, convexity and solidity were 100 % significant and the elongation variable in 75 % of cases was significant.

3.2.5. Multivariate analysis of variance (MANOVA)

According to the MANOVA's test values, the derived groups from cluster analysis do differ from each other regarding the four considered variables. The test was managed a 100-times. Results of the MANOVA yielded that there is a statistically significant difference between the three groups on the shape variables, repeated 100 times. The following indicators reflect the average of 100 repetitions:

$$\text{Wilks}'\ \lambda = 0.552, F(2, 1997) = 529.906, p < 0.001$$

although the visual interpretation of the plot on canonical variables from MANOVA suggests that the separation of groups 2nd and 3rd is incomplete (Fig. 9a).

Based on the MANOVA's statistical values related to fluvial and aeolian sediments, the classified sediments overlap (Fig. 9b), although, the multivariate test statistics support that the differences are statistically significant considering the four investigated variables in a hundredfold repetition. The following indicators reflect the average of 100 repetitions:

$$\text{Wilks}'\ \lambda = 0.910, F(2, 1097) = 36.243, p < 0.001$$

3.2.6. Principal component analysis (PCA)

Fig. 10a shows the scattergram of the first two principal components (PCs). PC1 explains 43 %, and PC2 explains 26 % of the total variance. The contribution of variables to the PCs is summarized in Table 2a. The HS circularity and convexity variables determine the PC1. The PC2 is defined by elongation and solidity parameters. The groups are separated by PC1, characterized by HS circularity and convexity. It means that groups are horizontally separated from each other. The 1st group has the most regular grains compared to the other two groups.

The diagram of Fig. 10b shows the scattergram of the first two PCs based on three morphological parameters of the fluvial and aeolian sediments. The first PC explains 46 %, and the second PC explains 28 % of the total variance. All three variables determine PC1. The PC2 is defined by solidity and convexity. The direction and length of the vectors indicate how each variable contributes to the two PCs. Based on that, the solidity variable defines and organizes the groups.

4. Discussion

General sedimentary processes like mechanical and chemical weathering, erosion and transportation as well as deposition control the form, the degree of roundness and the surface texture of mineral grains. Although, the geochemistry of the source area and the forces operating inside the rock (igneous, metamorphic, sedimentary) are the initial factors determining the shape of the sediment grains from which the form (elongation/sphericity/aspect ratio) may be preserved up to deposition (Cailleux, 1942; Scott and Smalley, 1991; Moss, 1966). The lithification and cementation of sediments also affect the morphological properties of grains by dissolving and crystallization of mineral components derived from chemical weathering and secondary quartz overgrowth (Pittman, 1972; Mazzullo and Megenheimer, 1987). The form of sedimentary grains depends largely on the physical properties of their source area because a spherical grain is less likely to break than an uneven particle of the same volume and physical properties and preferably break along their weakest incipient fractures (Moss, 1966). If angular features remain on the broken parts of a particle, they can be selectively reduced by further mechanical processes in any stress field, as the stress is preferentially concentrated on such features, thus achieving a rounding effect (Moss, 1966). Rounding generally occurs when the mechanically weathered grains prepared in the source area are of the appropriate size for the mode (rolling, saltation, suspension) and energy of transport. The mode of transport, the energy of the transport medium and the transport distance/time affect the rounding process besides the grain size and sorting. When gains are

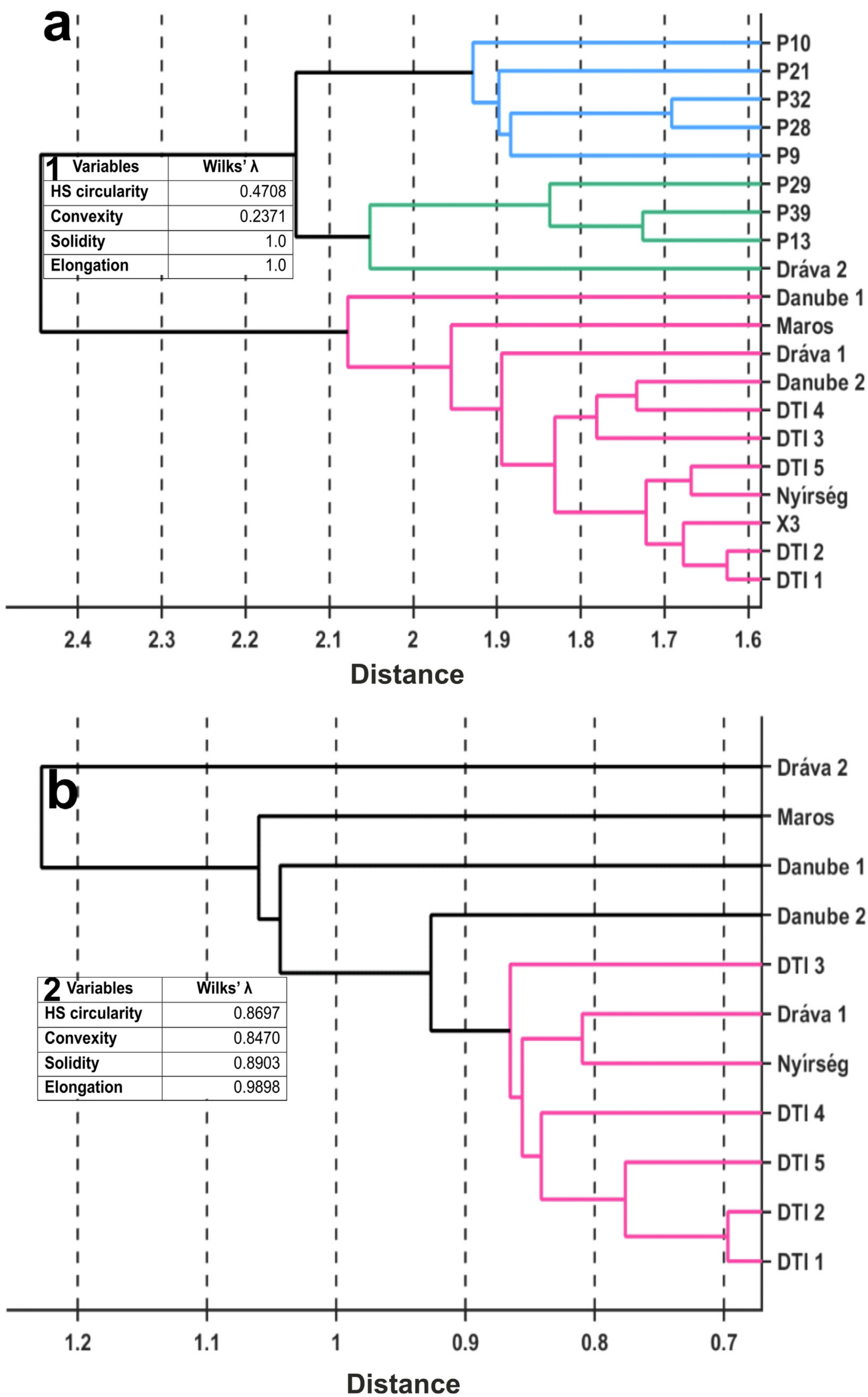

Fig. 6. a: Hierarchical cluster analysis of the investigated sedimentary environments based on four grain shape variables. b: Hierarchical cluster analysis of fluvial and aeolian sediments based on three grain shape variables. Pink = 1st group; green = 2nd group; black/blue = 3rd group. Tables: Wilks' λ values of the variables. HS circularity = high sensitivity circularity; DTI = Danube–Tisza Interfluve.

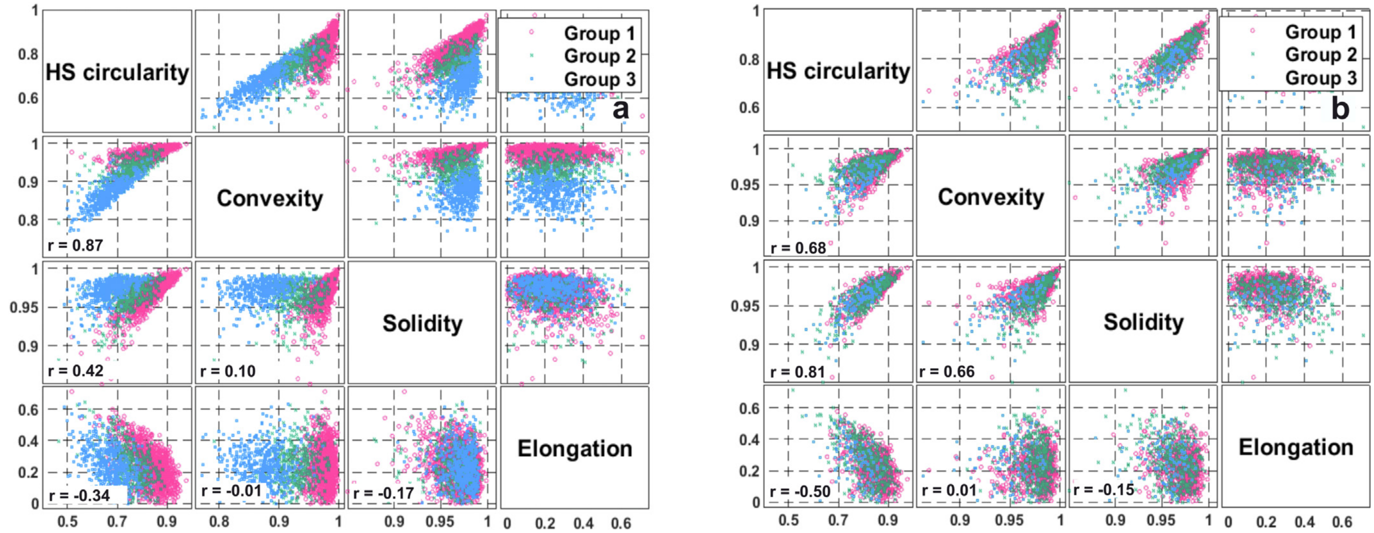

Fig. 7. a: Scatter plots of shape variables grouped by cluster analysis based on four grain shape variables. b: Scatter plot of shape variables grouped by cluster analysis of fluvial and aeolian sediments based on three grain shape variables. r = correlation coefficient. HS circularity = high sensitivity circularity.

transported relatively long distances, abrasion of the edges of the grains increases their roundness but does not alter their gross shape, the form (Mazzullo et al., 1986). Although, according to Chmielowska et al. (2021) the sphericity of the grains increases with the duration of the aeolian process and resulting in well-rounded grains which assumes that the initial shape is a freshly crushed grain. This is due to the randomness of the collisions between the grains. The most degradable parts of the grain surface, however, are the most distant fragments, which are leveled out one after the other during the collision. However, the shorter the period, the smaller the impact of the aeolian process (Mycielska-Dowgiałło and Woronko, 2004). In contrast, angular grain shape can result from the high-erosivity glacial environment (Mahaney, 2002), high-energy subaqueous environments (Helland and Holmes, 1997), or during random events such as tsunamis or storms (Costa et al., 2012a) that move the grains transported over a short period of time and their degree of roundness does not change. During grain-to-grain collisions, only the sharp edges of the grains are broken off (Chmielowska et al., 2021). In a fluvial environment the surface texture of quartz grains changes quickly without changing their roundness characteristics (Woronko et al., 2013; Woronko et al., 2015). In addition to the cases described so far, there are also cases and events where it is not possible to clearly identify which sedimentation process shapes the degree of roundness of the mineral grains. This means that grain characteristics can be directly inherited from previous sedimentation and original source area (Campaña et al., 2016; Chmielowska et al., 2021; Joo et al., 2018; Mazzullo et al., 1986; Mazzullo and Megenheimer, 1987; Sharp and Gomez, 1986; Suzuki et al., 2015; Tunwal et al., 2018; Woronko, 2016). Thus, the high degree of sphericity and/or roundness of aeolian or fluvial grains is not always a function of long-distance transport in successive environments (Chmielowska et al., 2021), therefore the grains can retain most of the properties inherited from their original environment if the transport distance is very short. In the Discussion section, we try to interpret the described controlling factors for our results.

4.1. Interpretation of the investigations with four shape parameters

Our initial results have given us a basic idea of the grain shape characteristics of our samples and their relationship to each other. Aeolian samples have more circular grains than fluvial deposits and sediments from the Kemeneshát. The X3 (Mogyoród) sample is similar to the aeolian samples if only the average values are considered. The floodplain sample (Dráva 2) has the lowest circularity and convexity characterization among fluvial and aeolian samples, resembling the P39 Kemeneshát sample. In general, the filling material of sand wedges is divided into two major groups in terms of circularity and convexity: (1) a group that contains relatively rounded, matured grains and (2) a unit that contains fresher grains.

Based on the analysis of the solidity modes of each sample, the fluvial sediments generally have lower values than both aeolian and sand wedge materials. Fluvial sediments differ from aeolian and infilling materials of sand wedges in terms of solidity. As for the elongation variable, although there are some outliers, it cannot be generalized that one kind of sediment typically has low or high elongation values. According to Sarkar et al. (2022), it is useful to investigate the grain shape based on the grain shape distribution curve because it gives additional information on the range of the different properties. In the words of Sarkar et al. (2022), the distribution curves can be described as "well-distributed" and "poorly distributed". Solidity values lie dominantly between 0.8 and 1, and HS circularity values can take values between 0.4 and 1.0. Aeolian samples have a narrower distribution of circularity values than the other two sediment types. That is why we classified the X3 (Mogyoród) sand wedge sample as aeolian sediment from the beginning of the exploration. Additionally, we noticed that fluvial materials have a broader distribution of solidity values compared to the other sediments. It is worth noting that the more rounded grains tend to have a narrower and leptokurtic distribution of solidity.

We applied a more detailed sediment analysis on 2000 individual grains (100 grains per sample) and repeated hundred times. The descriptive statistics gave similar results as the grain shape distribution analyses. The sand wedge materials can be distinguished by forming three groups. The X3 Mogyoród sample showed similarities to aeolian samples. Kemeneshát sediments form two separate groups, described as a fresh, less rounded sediment type (P9; P10; P21; P28; P32) and a more rounded, mature material (P13; P29; P39). The infilling material of sand wedges from Kemeneshát differentiates from aeolian and most of the fluvial samples. The Dráva 2 floodplain sediment showed similar characteristics to the regular, mature grains from Kemeneshát sediments. The elongation had the largest STD. After we applied hierarchical cluster analysis, the fluvial, aeolian and X3 (Mogyoród) samples were almost completely separated from the Kemeneshát samples. The Dráva 2 sediment was categorized among Kemeneshát sediments. The hypothesis was rejected in the case of HS circularity, convexity and solidity. Still, it could not be rejected in the case of elongation in the sense of the Kruskal–Wallis test. Based on the p-value from MANOVA, the certainty of the group means was below 1 %, considering the four

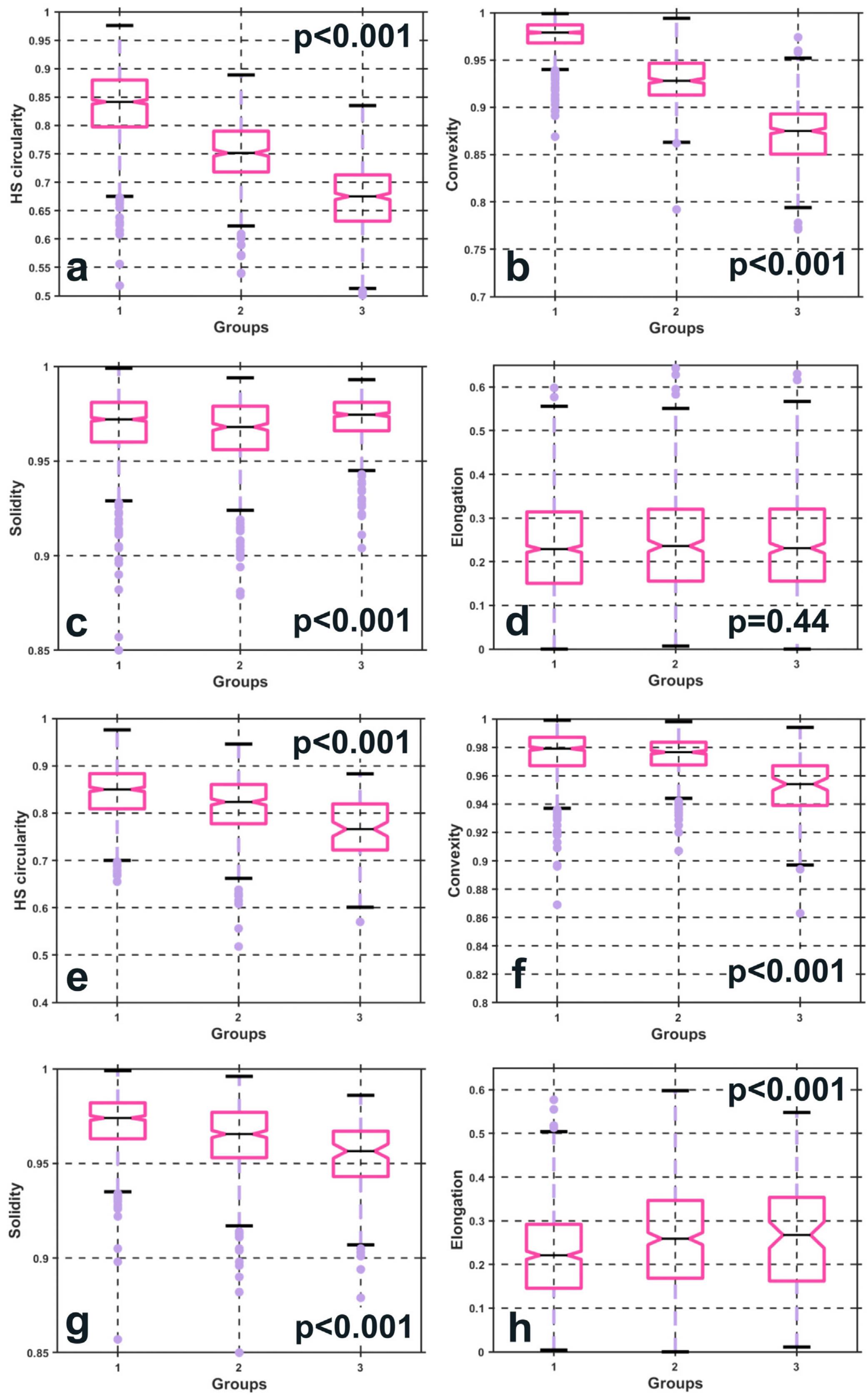

Fig. 8. a–d: Box plots of Kruskal–Wallis analysis based on four grain shape variables. e–h: Box plots of Kruskal–Wallis analysis of fluvial and aeolian sediments based on three grain shape variables. $\alpha = 0.05$. HS circularity = high sensitivity circularity.

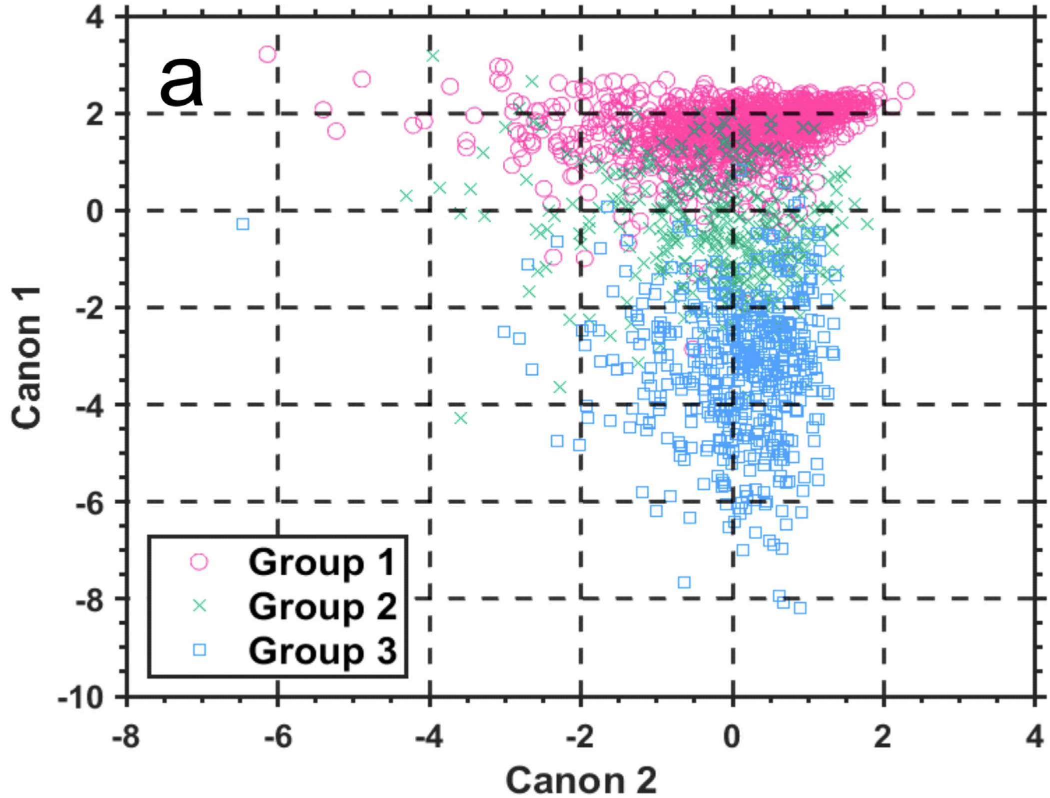

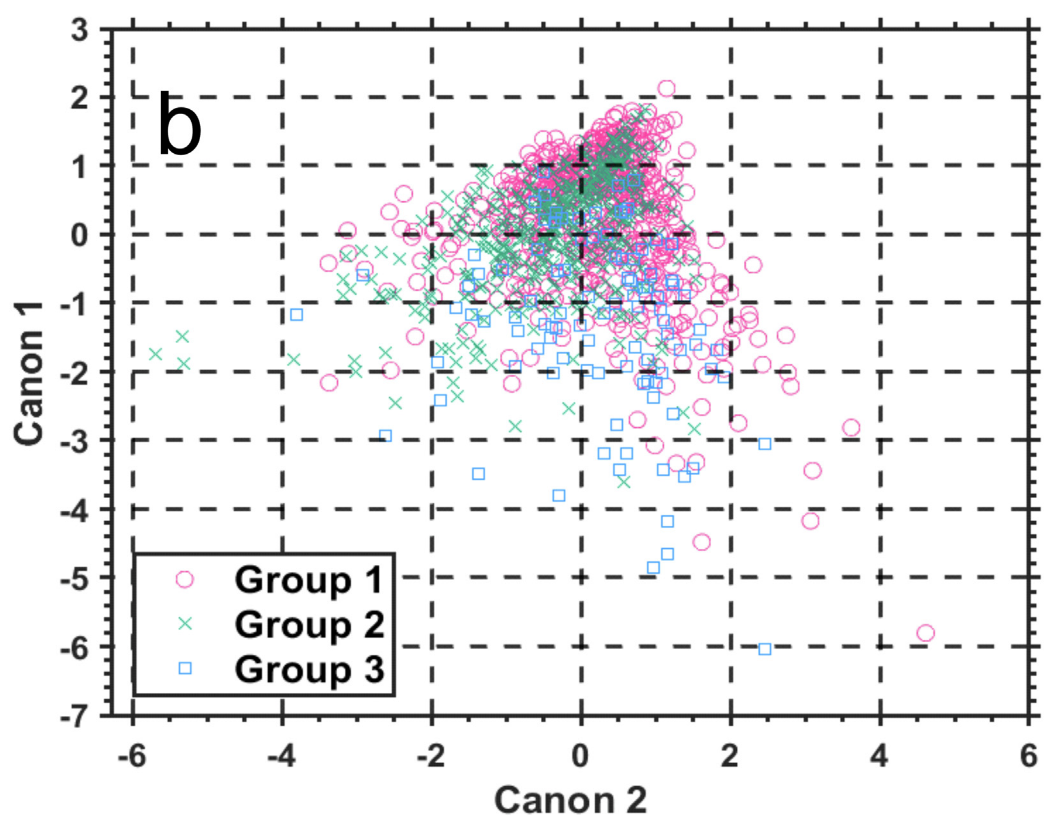

Fig. 9. a: Scatter plots of the first two canonical variables derived from MANOVA based on four variables. b: Scatter plot of the first two canonical variables of fluvial and aeolian sediments derived from MANOVA based on three grain shape variables. MANOVA = multivariate analysis of variance.

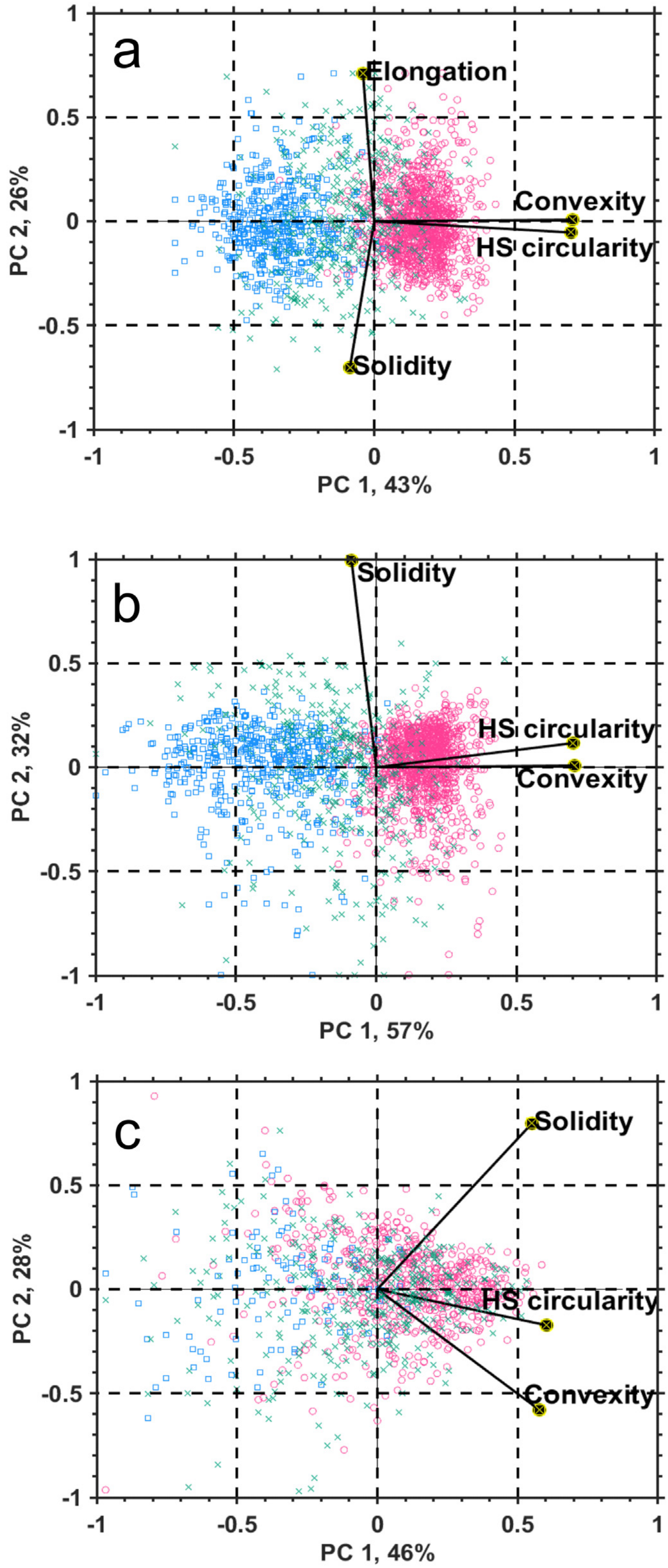

Fig. 10. a: Scatter plots of the first two PCs, which represent the directions and length of the four. b: Scatter plot of the first two PCs, which represents the directions and length of the three variables of fluvial and aeolian sediments. HS circularity = high sensitivity circularity; PC = principal component from PCA (principal component analysis).

investigated variables. Although, the visual idea of the groups on how they were located in the space revealed that the 2nd and 3rd groups were not separated. Some variables could be a stronger separate factor in some sediments. Wilks' λ results suggest that the circularity and

Table 2
Summary table of PCs, latent and explained variances. a: four variables; b: three variables of fluvial and aeolian sediments. PC = principal component from PCA (principal component analysis).

a	PC 1	PC 2	PC 3	PC 4
HS circularity	0.701	−0.053	0.109	−0.702
Convexity	0.706	0.007	0.016	0.707
Solidity	−0.086	−0.702	0.702	0.077
Elongation	−0.039	0.709	0.703	0.015
Latent	1.706	1.020	0.976	0.295
Explained (%)	42.66	25.52	24.42	7.3

b	PC 1	PC 2	PC 3
HS circularity	0.603	−0.172	0.778
Convexity	0.577	−0.579	−0.575
Solidity	0.550	0.796	−0.249
Latent	1.373	0.842	0.783
Explained (%)	45.78	28.091	26.126

convexity properties have a strong separation factor, which PCA supports because the groups separated along the first PC. Nevertheless, the lowest separating factor is elongation, which is understandable since this gives the largest STD within each sample. Therefore, elongation is the least powerful descriptor of our sample set regarding differentiating the sediment types, similar to Lipiec et al. (2016) and Szmańda and Witkowski (2021). In contrast, Suzuki et al. (2015) and Chmielowska et al. (2021) said that elongation/aspect ratio could distinguish the different sedimentary environments. Although Chmielowska et al. (2021) considered the elongation descriptor as a factor that can be used to monitor possible inheritance. The aspect of inheritance can be interpreted to the investigated fluvial sediments because the sphericity is relatively low, the solidity variable is also considered to be lower than the other analyzed sediments and the mean values of elongation are higher than aeolian. From this it can be deduced that since the form (elongation/aspect ratio) is the most difficult to change during sedimentary processes, they could all have inherited these traits from their source area since the roundness is relatively low. Although, the convexity (surface texture) was considered to be high which can be the result of the fluvial transportation (Woronko et al., 2013; Woronko et al., 2015). Fluvial and aeolian samples contain more spherical and rounded grains than the filling material of sand wedges from Kemeneshát. Although, among sand wedge samples, three main groups are described if we consider the X3 Mogyoród sample. The latter is the most rounded and spherical; therefore, it may have undergone a long transport process. The others are interpreted as a fresher group that did not spend much time in the transport medium. Although, even within these latter sediments, a more rounded, mature group exists.

According to Kovács et al. (2007), and based on grain shape characteristics, the X3 (Mogyoród) sand wedge sample tends to be originated from the surface allochthonous sand sediments considering the dominant westerly to north-westerly winds in winter during Late Pleniglacial in the central European region (Renssen et al., 2007). The deposition of the infilling sediment can be linked to the Pleistocene sand movement events from the last 25 ka at Danube–Tisza Interfluve (Gábris et al., 2012).

4.2. Identification of possible differences between fluvial and aeolian sediments

Many sedimentary geological studies and sedimentary environmental reconstructions deal with the problems of separation of fluvial and aeolian deposits. It is challenging to separate the two environments based on the granulometric fingerprints of the samples (for details, see Chmielowska et al., 2021 and references therein). We analyzed only aeolian and fluvial deposits (n = 11) without the sand wedge materials. We suspected in the previous results that the solidity variable could be the critical component in distinguishing these two types of sedimentary environments. We grouped the samples based on the preliminary result from hierarchical cluster analysis and Kruskal–Wallis. We separated the aeolian and fluvial samples from each other, although, Dráva 2 floodplain sediment formed a group on its own. There was minimal difference between the aeolian (1st group) and the main fluvial group (2nd group), but these differences were considered significant. The convexity variable caused the hierarchical cluster analysis to classify the fluvial groups into the aeolian groups in the previous investigations on all the sediments since the aeolian and fluvial samples show similarities regarding convexity. However, considering that the investigated aeolian materials are from a fluvial environment, the high convexity values may have been inherited from the former environment. The exception is maintained for the Dráva 2 sample (3rd group), which can be explained by the fact that this sample may have spent very little time in the transport medium because the convexity values did not change during this time. However, solidity had a more powerful influence on the separation of groups than before. Further investigation of PCA supported that solidity and HS circularity were the main components of separating the two sedimentary environments. Aeolian samples were more regular and compact, while the fluvial sediments had sharp edges and corners, which caused the solidity to be low. The sharp edges and corners were not chipped off during transport. Therefore, the low solidity (roundness) variable can be influenced by the too short transport or the low speed of the transport medium. The irregularity of the Dráva 2 sample is based on the HS circularity, convexity and solidity values. These variables were relatively low compared to the aeolian and the other fluvial group. Although, the aeolian and the main fluvial group had minimal differences regarding the convexity variable. These observations indicate that high HS circularity values are linked to the transport distance of sediments and the maturity of the grains (Campaña et al., 2016; Joo et al., 2018). In addition, the values determining roundness (convexity, solidity) are modified earlier than elongation, aspect ratio and circularity (Blott and Pye, 2008; Domokos et al., 2014; Campaña et al., 2016; Szmańda and Witkowski, 2021).

Based on our results using automated static image analysis, when the grain populations are relatively similar in roundness and surface texture, it is more difficult to identify their differences. At the same time, the interpretation of the results is more straightforward when comparing sediments with different levels of roundness, which was confirmed by several authors recently, like Altuhafi et al. (2013), Campaña et al. (2016), Joo et al. (2018), Chmielowska et al. (2021), and Szmańda and Witkowski (2021). Synchronously with Chmielowska et al. (2021), we found that convexity seems to have low sensitivity to identify grain edge roundness when comparing low circularity and high convexity (e.g., our fluvial sediments) with grains that have high circularity and convexity values (e.g., our aeolian samples) because they are seemingly similar. Regarding solidity, grains from fluvial sediments spent less time in the transport media or were transported at lower energy levels than aeolian grains because it can be expected that fluvial sands mature as downstream distances increase (Suzuki et al., 2015), but that relationship can only be observed slightly for Dráva 1 sediment. Therefore, the solidity values of fluvial sediments probably gave a more accurate description of the roundness of the grains, the transport distance and the energy level of the transportation. Thus, regarding transport energy and distance, the fluvial sediments were affected by relatively lower transportation energy but were transported for a longer distance than the infilling material of sand wedges. That is evidenced by the high solidity value of the sand wedge materials in contrast to the fluvial sediments' low solidity and high convexity values. We assume that the convexity property changed in a shorter period and transport distance (Woronko et al., 2013; Domokos et al., 2014; Woronko et al., 2015; Szmańda and Witkowski, 2021) and does not need a high-energy environment. However, high flow energy is required to detect changes in solidity values. Experimental studies showed that transport by wind is more effective in rounding sand-sized grains than transport by water (Kuenen, 1959, 1960; Mazzullo et al., 1986; Boggs Jr., 2014; Resentini et al., 2018). Therefore, we suggest that the infilling material of sand wedges from Kemeneshát went through at least two transportation mechanisms but spent a short time in the transport media because the grains have low circularity values, which means that that shape factor is inherited from the source. First, the grains were transported in water, and then the sediment was retrieved from the channel and temporarily deposited because the flow velocity and shear stress may have been decreased below the critical level required for sediment transport owing to a variety of causes, such as a decrease in the slope of the bed (topographical) and loss of water volume (seasonal or periodical, Vandenberghe and Woo, 2002; Attal and Lave, 2009; Boggs Jr., 2014). After temporary deposition, the high energy (periglacial environment, cold and dry climate) but short distance wind flow rounded the appropriately sized grains by increasing solidity values, which is related to a reduction of concavity. During grain-to-grain collisions, only the sharp edges of the grains are broken off (Chmielowska et al., 2021). The wind then deposited the grains into the open frost cracks, acting as sediment traps. The low convexity values can be explained by the repeated frost weathering related to the periglacial climatic conditions (Górska and Woronko, 2022; Górska et al., 2022) since quartz grains in such environment are susceptible to chemical and physical abrasion, which can lead to the irregular shape. However, we also have a less complex theory, namely, that the high-energy (e.g., steep river environments, energetic collisions) aqueous environment rounded the concave grains at a short distance (Attal and Lave, 2009; Domokos et al., 2014; Joo et al., 2018). The wind probably did not play an important role in rounding the grains, and it only played a part in depositing the grains into the frost wedges. After deposition, the grains lost their high convexity values because of frost abrasion.

5. Conclusions

Investigating grain shape parameters of different sediment types using the Malvern Morphologi G3SE-ID device proved to be highly effective. Our study revealed that distinguishing between geomorphological environments in the Carpathian Basin is possible based on sediment grains' high sensitivity (HS) circularity, convexity and solidity parameters. Since we have only studied Carpathian Basin sediments, it is not yet possible to generalize our findings and the results of our investigations to all types of dunes and fluvial deposits. Although, our investigation can serve as a reference for analyzing similar sedimentary deposits in other regions.

According to univariate and multivariate statistics, HS circularity and convexity are the most effective attributes distinguishing the depositional environments, mainly the fluvial and aeolian environments, from the infilling material of sand wedges. That seemed much easier compared to remarkably different levels of roundness and form. The elongation variable was the least influential parameter in distinguishing sedimentary environments. The high HS circularity values can indicate a longer transport distance. In contrast, the high solidity factors can be used to identify the high-transport energy and long transport distance. In a fluvial environment the convexity variable can change in relatively low energy and short time. Although, it is important to take into account that the analyzed variables do not reflect the actual conditions of the environment. Low HS circularity and low roundness (solidity) factors can reflect the source area's initial conditions and the energy transport medium was not enough to chip the edges of the grains. Low HS circularity and high solidity can indicate that the energy of the transport medium was high enough to break the concave edges of the mineral grains, but the transport distance was not long enough to smooth their edges. Furthermore, if one of the other shape parameters is not in harmony with the others, it may indicate a post-depositional process, such as high solidity accompanied by low convexity.

The infilling materials of sand wedges from Kemeneshát underwent at least two transport processes: a high-energy aqueous, a wind transport mechanism, and possibly a post-depositional alteration process (frost weathering).

The solidity parameter proved to be an effective variable in separating sediments with similar convexity values, which were – in our case – the aeolian and fluvial environments. Fluvial sediments from Maros, Dráva and Danube had lower solidity values which resembles that these sediments are not as much rounded as aeolian sands from Nyírség and Danube–Tisza Interfluve. Our research supports the previously established theory that aeolian transport is more effective in rounding the grains than in an aqueous environment.

This study also faced some limitations that must be acknowledged. The primary objective of our paper was to present a new depositional environment reconstruction method based on granulometric parameters of a large number of individual grains and multivariate mathematical–statistical analyses. This paper presents the new procedure only by analyzing a few local samples considered representative of different main depositional processes. The selected samples are from well-distinguishable sedimentary environments. In fact, even for just one typical environment (fluvial, aeolian, lacustrine, etc.), several sub-processes may play a role in forming the granulometric fingerprints. Still, the primary objective of this paper was to introduce the method, not to provide a detailed paleoenvironmental reconstruction of one section or site.

It could be necessary to define further the boundaries of the shape parameters and what environmental effects specific values may indicate. That requires analyzing as many recent and past sediments as possible to record their grain shape properties. Our research can support paleogeographical reconstruction studies by investigating paleo and recent sediments. Recent sediments with known environmental and geographical conditions can facilitate the interpretation of paleoenvironmental conditions. By understanding the past, we can predict the potential impact of future environmental conditions.

Supplementary data to this article can be found online at https://doi.org/10.1016/j.sedgeo.2023.106479.

Data availability

Datasets related to this article can be found at https://data.mendeley.com/datasets/p78zbnk6sb/draft?a=20dcb95f-bae9-44dd-a4a7-29b8f99c0588 an open-source online data repository hosted at Mendeley Data.

Declaration of competing interest

The authors declare that they have no known competing financial interests or personal relationships that could have appeared to influence the work reported in this paper.

Acknowledgment

Supports of the National Research, Development and Innovation Fund Office (Hungary) under contract NKFIH FK138692 and RRF-2.3.1-21-2022-00014 National Multidisciplinary Laboratory for Climate Change are gratefully acknowledged. We would like to thank the reviewers for their valuable input, which helped improving the overall quality of the manuscript.

References

Altuhafi, F., O'Sullivan, C., Cavarretta, I., 2013. Analysis of an image-based method to quantify the size and shape of sand particles. Journal of Geotechnical and Geoenvironmental Engineering 139, 1290–1307.

Attal, M., Lave, J., 2009. Pebble abrasion during fluvial transport: experimental results and implications for the evolution of the sediment load along rivers. Journal of Geophysical Research - Earth Surface 114, 1–22.

Barrett, P.J., 1980. The shape of rock particles, a critical review. Sedimentology 27, 291–303.

Battarbee, R.W., Jones, V.J., Flower, R.J., Cameron, N.G., Bennion, H., 2001. Diatoms. In: Smol, J.P., Birks, H.J.B., Last, W.M. (Eds.), Tracking Environmental Change Using Lake Sediments: Terrestrial, Algal and Siliceous Indicators. vol. 3. Kluwer Academic Publishers, Dordrecht, pp. 155–202.

Beuselinck, L., Govers, G., Poesen, J., Degraer, G., Froyen, L., 1998. Grain-size analysis by laser diffractometry: comparison with the sieve-pipette method. CATENA 32, 193–208.

Bieganowski, A., Ryżak, M., Sochan, A., Barna, G., Hernádi, H., Beczek, M., Polakowski, C., Makó, A., 2018. Laser diffractometry in the measurements of soil and sediment particle size distribution. Advances in Agronomy 151, 215–279.

Bittelli, M., Andrenelli, M.C., Simonetti, G., Pellegrini, S., Artioli, G., Piccoli, I., Morari, F., 2019. Shall we abandon sedimentation methods for particle size analysis in soils? Soil and Tillage Research 185, 36–46.

Black, R.F., 1976. Periglacial features indicative of permafrost: ice and soil wedges. Quaternary Research 6, 3–26.

Blott, S.J., Pye, K., 2008. Particle shape: a review and new methods of characterization and classification. Sedimentology 55, 31–63.

Boggs Jr., S., 2014. Principles of Sedimentology and Stratigraphy. 5th edition. Pearson Education Limited, Edinburgh Gate, Harlow, Essex (560 pp.).

Bull, W.B., 1962. Relation of textural (CM) patterns to depositional environment of alluvial-fan deposits. SEPM Journal of Sedimentary Research 32, 211–216.

Buró, B., Sipos, Gy, Lóki, J., Andrási, B., Félegyházi, E., Négyesi, G., 2016. Assessing Late Pleistocene and Holocene phases of aeolian activity on the Nyírség alluvial fan, Hungary. Quaternary International 425, 183–195.

Cailleux, A., 1942. Les actiones eoliennes periglaciaires en Europe. Mémoires de la Société géologique de France. Paléontologie. 41, 1–176 (in French).

Campaña, I., Benito-Calvo, A., Pérez-González, A., Bermúdez de Castro, J.M., Carbonell, E., 2016. Assessing automated image analysis of sand grain shape to identify sedimentary facies, Gran Dolina archaeological site (Burgos, Spain). Sedimentary Geology 346, 72–83.

Chmielowska, D., Woronko, B., Dorocki, S., 2021. Applicability of automatic image analysis in quartz-grain shape discrimination for sedimentary setting reconstruction. CATENA 207, 105602. https://doi.org/10.1016/j.catena.2021.105602.

Cosgrove, G.I.E., Hodgson, D.M., Poyatos-Moré, M., Mountney, N.P., McCaffrey, W.D., 2018. Filter or conveyor? Establishing relationships between clinoform rollover trajectory, sedimentary process regime, and grain character within intrashelf clinothems, offshore New Jersey, U.S.A. Journal of Sedimentary Research 88, 917–941.

Costa, P.J.M., Andrade, C., Dawson, A.G., Mahaney, W.C., Freitas, M.C., Paris, R., Taborda, R., 2012a. Microtextural characteristics of quartz grains transported and deposited by tsunamis and storms. Sedimentary Geology 275–276, 55–69.

Costa, P.J.M., Andrade, C., Freitas, M.C., Oliveira, M.A., Lopes, V., Dawson, A.G., Moreno, J., Fatela, F., Jouanneau, J.M., 2012b. A tsunami record in the sedimentary archive of the central Algarve coast, Portugal: characterizing sediment, reconstructing sources and inundation paths. Holocene 22, 899–914.

Costa, P.J.M., Andrade, C., Mahaney, W.C., Marques da Silva, F., Freire, P., Freitas, M.C., Janardo, C., Oliveira, M.A., Silva, T., Lopes, V., 2013. Aeolian microtextures in silica spheres induced in a wind tunnel experiment: comparison with aeolian quartz. Geomorphology 180–181, 120–129.

Cox, E., 1927. A method of assigning numerical and percentage values to the degree of roundness of sand grains. Journal of Paleontology 1, 179–183.

Cox, M.R., Budhu, M., 2008. A practical approach to grain shape quantification. Engineering Geology 96, 1–16.

Di Stefano, C., Ferro, V., Mirabile, S., 2010. Comparison between grain-size analyses using laser diffraction and sedimentation methods. Biosystems Engineering 106, 205–215.

Dietze, E., Hartmann, K., Diekmann, B., IJmker, J., Lehmkuhl, F., Opitz, S., Stauch, G., Wünnemann, B., Borchers, A., 2012. An end-member algorithm for deciphering modern detrital processes from lake sediments of Lake Donggi Cona, NE Tibetan Plateau, China. Sedimentary Geology 243–244, 169–180.

Doeglas., D.J., 1946. Interpretation of the results of mechanical analyses. SEPM Journal of Sedimentary Research 16, 19–40.

Domokos, G., Jerolmack, D.J., Sipos, A.Á., Török, Á., 2014. How river rocks round: resolving the shape-size paradox. PLoS One 9, 1–7.

Dövényi, Z., 2010. Magyarország Kistájainak Katasztere. 2nd edition. MTA Földrajztudományi Kutatóintézet, Budapest (876 pp., in Hungarian).

Fábián, S.Á., Kovács, J., Varga, G., Sipos, G., Horváth, Z., Thamó-Bozsó, E., Tóth, G., 2014. Distribution of relict permafrost features in the Pannonian Basin, Hungary. Boreas 43, 722–732.

Farkas, B., Sipos, G., Bartyik, T., Józsa, E., Czigány, Sz, Balogh, R., Varga, G., Kovács, J., Fábián, S.A., 2023. Characterization and mapping of MIS-2 thermal contraction crack polygons in Western Transdanubia, Hungary. Permafrost and Periglacial Processes, 1–11 https://doi.org/10.1002/ppp.2190.

Fitzpatrick, K., Summerson, C., 1971. Some observations on electron micrographs of quartz sand grains. The Ohio Journal of Science 71, 106–119.

Folk, R.L., 1955. Student operator error in determination of roundness, sphericity, and grain size. Journal of Sedimentary Petrology 25, 297–301.

Friedman, G.M., 1961. Distinction between dune, beach and river sands from their textural characteristics. Journal of Sedimentary Petrology 31, 514–529.

Gábris, G., Horváth, E., Novothny, Á., Ruszkiczay-Rüdiger, Z., 2012. Fluvial and aeolian landscape evolution in Hungary - results of the last 20 years research. Geologie en Mijnbouw/Netherlands Journal Geosciences 91, 111–128.

Górska, M.E., Woronko, B., 2022. Multi-stage evolution of frost-induced microtextures on the surface of quartz grains—an experimental study. Permafrost and Periglacial Processes 33, 3–9.

Górska, M.E., Woronko, B., Kossowski, T.M., Pisarska-Jamroży, M., 2022. Micro-scale frost-weathering simulation – changes in grain-size composition and influencing factors. CATENA 212, 106106. https://doi.org/10.1016/j.catena.2022.106106.

Gray, A.B., Pasternack, G.B., Watson, E.B., 2009. Hydrogen peroxide treatment effects on the particle size distribution of alluvial and marsh sediments. The Holocene 20, 293–301.

Greenwood, B., 1969. Sediment parameters and environment discrimination: an application of multivariate statistics. Canadian Journal of Earth Sciences 6, 1347–1358.
Gresina, F., 2020. Comparison of pipette method and state of the art analytical techniques to determine granulometric properties of sediments and soils. Hungarian Geographical Bulletin 69, 27–39.
Helland, P.E., Holmes, M.A., 1997. Surface textural analysis of quartz sand grains from ODP site 918 off the southeast coast of Greenland suggests glaciation of southern Greenland at 11 Ma. Palaeogeography, Palaeoclimatology, Palaeoecology 135, 109–121.
Ijmker, J., Stauch, G., Dietze, E., Hartmann, K., Diekmann, B., Lockot, G., Opitz, S., Wünnemann, B., Lehmkuhl, F., 2012. Characterisation of transport processes and sedimentary deposits by statistical end-member mixing analysis of terrestrial sediments in the Donggi Cona lake catchment, NE Tibetan Plateau. Sedimentary Geology 281, 166–179.
Joo, Y.J., Soreghan, A.M., Madden, M.E.E., Soreghan, G.S., 2018. Quantification of particle shape by an automated image analysis system: a case study in natural sediment samples from extreme climates. Geosciences Journal 22, 525–532.
Kalińska, E., Lamsters, K., Karušs, J., Krievāns, M., Rečs, A., Ješkins, J., 2022. Does glacial environment produce glacial mineral grains? Pro- and supra-glacial Icelandic sediments in microtextural study. Quaternary International 617, 101–111.
Kalińska-Nartiša, E., Stivrins, N., Grudzinska, I., 2018. Quartz grains reveal sedimentary palaeoenvironment and past storm events: a case study from eastern Baltic. Estuarine, Coastal and Shelf Science 200, 359–370.
Katra, I., Yizhaq, H., 2017. Intensity and degree of segregation in bimodal and multimodal grain size distributions. Aeolian Research 27, 23–34.
Keller, W.D., 1945. Size distribution of sand in some dunes, beaches, and sandstones. AAPG Bulletin 29, 215–221.
Király, C., Falus, G., Gresina, F., Jakab, G., Szalai, Z., Varga, G., 2019. Granulometric properties of particles in Upper Miocene sandstones from thin sections, Szolnok Formation, Hungary. Hungarian Geographical Bulletin 68, 341–353.
Kok, J.F., Parteli, E.J.R., Michaels, T.I., Karam, D.B., 2012. The physics of wind-blown sand and dust. Reports on Progress in Physics 75, 106901. https://doi.org/10.1088/0034-4885/75/10/106901.
Konert, M., Vandenberghe, J., 1997. Comparison of laser grain size analysis with pipette and sieve analysis: a solution for the underestimation of the clay fraction. Sedimentology 44, 523–535.
Kovács, J., Fábián, S.Á., Schweitzer, F., Varga, G., 2007. A relict sand-wedge polygon site in north-central Hungary. Permafrost and Periglacial Processes 18, 379–384.
Krauß, L., Zens, J., Zeeden, C., Schulte, P., Eckmeier, E., Lehmkuhl, F., 2016. A multi-proxy analysis of two loess-paleosol sequences in the Northern Harz Foreland, Germany. Palaeogeography, Palaeoclimatology, Palaeoecology 461, 401–417.
Krinsley, D., Wellendorf, W., 1980. Wind velocities determined from the surface textures of sand grains. Nature 283, 372–373.
Krumbein, W.C., 1941. Measurement and geological significance of shape and roundness of sedimentary particles. SEPM Journal of Sedimentary Research 11, 64–72.
Kuenen, P.H., 1959. Experimental abrasion: 3, fluviatile action on sand. American Journal of Science 257, 172–190.
Kuenen, P.H., 1960. Experimental abrasion 4: eolian action. Journal of Geology 68, 427–449.
Kuenen, H., Perdok, W.G., 1962. Experimental abrasion 5. Frosting and defrosting of quartz grains. Journal of Geology 70, 648–658.
Lewin, J., Brewer, P.A., 2002. Laboratory simulation of clast abrasion. Earth Surface Processes and Landforms 27, 145–164.
Lipiec, J., Siczek, A., Sochan, A., Bieganowski, A., 2016. Effect of sand grain shape on root and shoot growth of wheat seedlings. Geoderma 265, 1–5.
Lóki, J., Hertelendi, E., Borsy, Z., 1994. New dating of blown sand movement in the Nyírség. Acta Geographica Debrecina 32, 67–76.
MacCarthy, G.R., 1935. Eolian sands, comparison. American Journal of Science 30, 81–95.
Mahaney, W.C., 2002. Atlas of Sand Grain Surface Textures and Applications. Oxford University Press, Oxford, p. 237.
Mahaney, W.C., Andres, W., 1990. Glacially crushed quartz grains in loess as indicators of long-distance transport from major European ice centers during the Pleistocene. Palaeogeography, Palaeoclimatology, Palaeoecology 121, 89–103.
Mahaney, W.C., Dohm, J.M., 2011. The 2011 Japanese 9.0 magnitude earthquake: test of a kinetic energy wave model using coastal configuration and offshore gradient of Earth and beyond. Sedimentary Geology 239, 80–86.
Martewicz, J., Kalińska, E., Weckwerth, P., 2022. What hides in the beach sand? A multiproxy approach and new textural code to recognition of beach evolution on the southern and eastern Baltic Sea coast. Sedimentary Geology 435, 106154. https://doi.org/10.1016/j.sedgeo.2022.106154.
Mazzullo, J., Megenheimer, S., 1987. The original shapes of quartz sand grains. Journal of Sedimentary Petrology 57, 479–487.
Mazzullo, J.I.M., Sims, D., Cunningham, D., 1986. The effects of eolian sorting and abrasion upon the shapes of fine quartz sand grains. Journal of Sedimentary Research 56, 45–56.
Middleton, G.V., 1976. Hydraulic interpretation of sand size distributions. Journal of Geology 84, 405–426.
Moss, A.J., 1966. Origin, shaping and significance of quartz sand grains. Journal of the Geological Society of Australia 13, 97–136.
Murton, J.B., Worsley, P., Gozdzik, J., 2000. Sand veins and wedges in cold aeolian environments. Quaternary Science Reviews 19, 899–922.
Mycielska-Dowgiałło, E., Woronko, B., 2004. The degree of aeolization of Quaternary deposits in Poland as a tool for stratigraphic interpretation. Sedimentary Geology 168, 149–163.
Parris, A.S., Bierman, P.R., Noren, A.J., Prins, M.A., Lini, A., 2010. Holocene paleostorms identified by particle size signatures in lake sediments from the northeastern United States. Journal of Paleolimnology 43, 29–49.
Passega, R., Byramjee, R., 1969. Grain-size image of clastic deposits. Sedimentology 13, 233–252.
Patro, B.C., Sahu, B.K., 1977. Discriminant analysis of sphericity and roundness data of clastic quartz grains in rivers, beaches and dunes. Sedimentary Geology 19, 301–311.
Pittman, E.D., 1972. Diagenesis of quartz in sandstones as revealed by scanning electron microscopy. Journal of Sedimentary Petrology 42, 507–546.
Powers, M.C., 1953. A new roundness scale for sedimentary particles. Journal of Sedimentary Research 23, 117–119.
Prins, M.A., Vriend, M., Nugteren, G., Vandenberghe, J., Lu, H., Zheng, H., Jan Weltje, G., 2007. Late Quaternary aeolian dust input variability on the Chinese Loess Plateau: inferences from unmixing of loess grain-size records. Quaternary Science Reviews 26, 230–242.
Pye, K., 1995. The nature, origin and accumulation of loess. Quaternary Science Reviews 4, 653–667.
Renssen, H., Kasse, C., Vandenberghe, J., Lorenz, S.J., 2007. Weichselian Late Pleniglacial surface winds over northwest and central Europe: a model-data comparison. Journal of Quaternary Science 22, 281–293.
Resentini, A., Andò, S., Garzanti, E., 2018. Quantifying roundness of detrital minerals by image analysis: sediment transport, shape effects, and provenance implications. Journal of Sedimentary Research 88, 276–289.
Riley, N.A., 1941. Projection sphericity. Journal of Sedimentary Research 11, 94–97.
Rostási, Á., Topa, B.A., Gresina, F., Weiszburg, T.G., Gelencsér, A., Varga, G., 2022. Saharan dust deposition in central Europe in 2016—a representative year of the increased North African dust removal over the last decade. Frontiers in Earth Science 10, 1–18.
Rousseau, D.D., Antoine, P., Hatté, C., Lang, A., Zöller, L., Fontugne, M., Othman, D. Ben, Luck, J.M., Moine, O., Labonne, M., Bentaleb, I., Jolly, D., 2002. Abrupt millennial climatic changes from Nussloch (Germany) Upper Weichselian eolian records during the Last Glaciation. Quaternary Science Reviews 21, 1577–1582.
Ruszkiczay-Rüdiger, Zs, Dunai, T.J., Bada, G., Fodor, L., Horváth, E., 2005. Middle to late Pleistocene uplift rate of the Hungarian Mountain Range at the Danube Bend, (Pannonian Basin) using in situ produced ^{3}He. Tectonophysics 410, 173–187.
Sarkar, D., Goudarzy, M., Wichtmann, T., 2022. Inspection of various grain morphology parameters based on wave velocity measurements on three different granular materials. Soil Dynamics and Earthquake Engineering 153, 107071. https://doi.org/10.1016/j.soildyn.2021.107071.
Schulte, P., Sprafke, T., Rodrigues, L., Fitzsimmons, K.E., 2018. Are fixed grain size ratios useful proxies for loess sedimentation dynamics? Experiences from Remizovka, Kazakhstan. Aeolian Research 31, 131–140.
Scott, C., Smalley, I., 1991. The original shapes of quartz sand grains. Royal Geographical Society 23, 353–355.
Shang, Y., Kaakinen, A., Beets, C.J., Prins, M.A., 2018. Aeolian silt transport processes as fingerprinted by dynamic image analysis of the grain size and shape characteristics of Chinese loess and Red Clay deposits. Sedimentary Geology 375, 36–48.
Sharp, M., Gomez, B., 1986. Processes of debris comminution in the glacial environment and implications for quarts sand-grain micromorphology. Sedimentary Geology 46, 33–47.
Smalley, I.J., Kumar, R., O'Hara, Dhand K., Jefferson, I.F., Evans, R.D., 2005. The formation of silt material for terrestrial sediments: particularly loess and dust. Sedimentary Geology 179, 321–328.
Sneed, E.D., Folk, R.L., 1958. Pebbles in the Lower Colorado River, Texas a study in particle morphogenesis. Journal of Geology 66, 114–150.
Sochan, A., Zieliński, P., Bieganowski, A., 2015. Selection of shape parameters that differentiate sand grains, based on the automatic analysis of two-dimensional images. Sedimentary Geology 327, 14–20.
Somogyi, S., 1962. A Vasi-Hegyhát és a Kemeneshát. Földrajzi Értesítő 12, 52–60 (in Hungarian).
Sun, D., Bloemendal, J., Rea, D., Vandenberghe, J., Jiang, F., An, Z., Su, R., 2002. Grain-size distribution function of polymodal sediments in hydraulic and aeolian environments, and numerical partitioning of the sedimentary components. Sedimentary Geology 152, 263–277.
Sun, D., Bloemendal, J., Rea, D.K., Zhisheng, A., Vandenberghe, J., Huayu, L., Ruixia, S., Tungsheng, L., 2004. Bimodal grain-size distribution of Chinese loess and its paleoclimatic implications. CATENA 55, 325–340.
Suzuki, K., Fujiwara, H., Ohta, T., 2015. The evaluation of macroscopic and microscopic textures of sand grains using elliptic Fourier and principal component analysis: implications for the discrimination of sedimentary environments. Sedimentology 62, 1184–1197.
Szmańda, J.B., Witkowski, K., 2021. Morphometric parameters of Krumbein grain shape charts—a critical approach in light of the automatic grain shape image analysis. Minerals 11, 937. https://doi.org/10.3390/min11090937.
Tafesse, S., Robison Fernlund, J.M., Sun, W., Bergholm, F., 2013. Evaluation of image analysis methods used for quantification of particle angularity. Sedimentology 60, 1100–1110.
Taubner, H., Roth, B., Tippkötter, R., 2009. Determination of soil texture: comparison of the sedimentation method and the laser-diffraction analysis. Journal of Plant Nutrition and Soil Science 172, 161–171.
Tunwal, M., Mulchrone, K.F., Meere, P.A., 2018. Quantitative characterization of grain shape: implications for textural maturity analysis and discrimination between depositional environments. Sedimentology 65, 1761–1776.
Udden, J.A., 1914. Mechanical composition of clastic sediments. Bulletin of the Geological Society of America 25, 655–744.
Újvári, G., Kok, J.F., Varga, G., Kovács, J., 2016. The physics of wind-blown loess: implications for grain size proxy interpretations in Quaternary paleoclimate studies. Earth-Science Reviews 154, 247–278.
Vaasma, T., 2008. Grain-size analysis of lacustrine sediments: a comparison of pretreatment methods: Estonian. Journal of Ecology 57, 231–243.

van Hateren, J.A., Prins, M.A., van Balen, R.T., 2018. On the genetically meaningful decomposition of grain-size distributions: a comparison of different end-member modelling algorithms. Sedimentary Geology 375, 49–71.
van Hateren, J.A., van Buuren, U., Arens, S.M., van Balen, R.T., Prins, M.A., 2020. Identifying sediment transport mechanisms from grain size-shape distributions. Earth Surface Dynamics 8, 527–553.
Vandenberghe, J., 2013. Grain size of fine-grained windblown sediment: a powerful proxy for process identification. Earth-Science Reviews 121, 18–30.
Vandenberghe, J., Nugteren, G., 2001. Rapid climatic changes recorded in loess successions. Global and Planetary Change 28, 1–9.
Vandenberghe, J., Pissart, A., 1993. Permafrost changes in Europe during the last glacial. Permafrost and Periglacial Processes 4, 121–135.
Vandenberghe, J., Woo, M.K., 2002. Modern and ancient periglacial river types. Progress in Physical Geography 26, 479–506.
Vandenberghe, J., An, Z.S., Nugteren, G., Lu, H., van Huissteden, J., 1997. New absolute time scale for the Quaternary climate in the Chinese loess region by grain-size analysis. Geology 25, 35–38.
Varga, G., Roettig, C.B., 2018. Identification of Saharan dust particles in Pleistocene dune sand-paleosol sequences of Fuerteventura (Canary Islands). Hungarian Geographical Bulletin 67, 121–141.
Varga, G., Cserháti, C., Kovács, J., Szalai, Z., 2016. Saharan dust deposition in the Carpathian Basin and its possible effects on interglacial soil formation. Aeolian Research 22, 1–12.
Varga, G., Kovács, J., Szalai, Z., Cserháti, C., Újvári, G., 2018. Granulometric characterization of paleosols in loess series by automated static image analysis. Sedimentary Geology 370, 1–14.
Varga, G., Gresina, F., Újvári, G., Kovács, J., Szalai, Z., 2019a. On the reliability and comparability of laser diffraction grain size measurements of paleosols in loess records. Sedimentary Geology 389, 42–53.
Varga, G., Újvári, G., Kovács, J., 2019b. Interpretation of sedimentary (sub)populations extracted from grain size distributions of Central European loess-paleosol series. Quaternary International 502, 60–70.
Varga, G., Dagsson-Waldhauserová, P., Gresina, F., Helgadottir, A., 2021. Saharan dust and giant quartz particle transport towards Iceland. Scientific Reports 11, 11891. https://doi.org/10.1038/s41598-021-91481-z.
Visher, G.S., 1969. Grain size distributions and depositional processes. Journal of Sedimentary Petrology 39, 1074–1106.
Vos, K., Vandenberghe, N., Elsen, J., 2014. Surface textural analysis of quartz grains by scanning electron microscopy (SEM): from sample preparation to environmental interpretation. Earth-Science Reviews 128, 93–104.
Wadell, H., 1932. Volume, shape, and roundness of rock particles. Journal of Geology 40, 443–451.
Wadell, H., 1935. Volume, shape, and roundness of quartz particles. Journal of Geology 43, 250–280.
Walling, D.E., 2013. The evolution of sediment source fingerprinting investigations in fluvial systems. Journal of Soils and Sediments 13, 1658–1675.
Wentworth, C.K., 1919. A laboratory and field study of cobble abrasion. Journal of Geology 27, 507–521.
Wentworth, C.K., 1922. The shapes of beach pebbles. Professional Paper US. Geological Surveyvol. 131C, pp. 75–83.
Woronko, B., 2016. Frost weathering versus glacial grinding in the micromorphology of quartz sand grains: processes and geological implications. Sedimentary Geology 335, 103–119.
Woronko, B., Pisarska-Jamrozy, M., 2016. Micro-scale frost weathering of sand-sized quartz grains. Permafrost and Periglacial Processes 27, 109–122.
Woronko, B., Rychel, J., Karasiewicz, M.K., Ber, A., Krzywicki, T., Marks, L., Pochocka-Szwarc, K., 2013. Heavy and light minerals as a tool for reconstructing depositional environments: an example from the Jałówka site (northern Podlasie region, NE Poland). Geologos 19, 47–66.
Woronko, B., Pisarska-Jamroży, M., van Loon, A.J., 2015. Reconstruction of sediment provenance and transport processes from the surface textures of quartz grains from Late Pleistocene sandurs and an ice-marginal valley in NW Poland. Geologos 21, 105–115.
Xu, Y., Li, J., Pan, F., Yang, B., Tang, Y., Bi, Y., Li, T., Yue, L., Wingate, M.T.D., 2018. Late Neogene aridification and wind patterns in the Asian interior: insight from the grain-size of eolian deposits in Altun Shan, northern Tibetan Plateau. Palaeogeography Palaeoclimatology Palaeoecology 511, 532–540.